iScience

CellPress
OPEN ACCESS

Article

Emx2 is an essential regulator of ciliated cell development across embryonic tissues

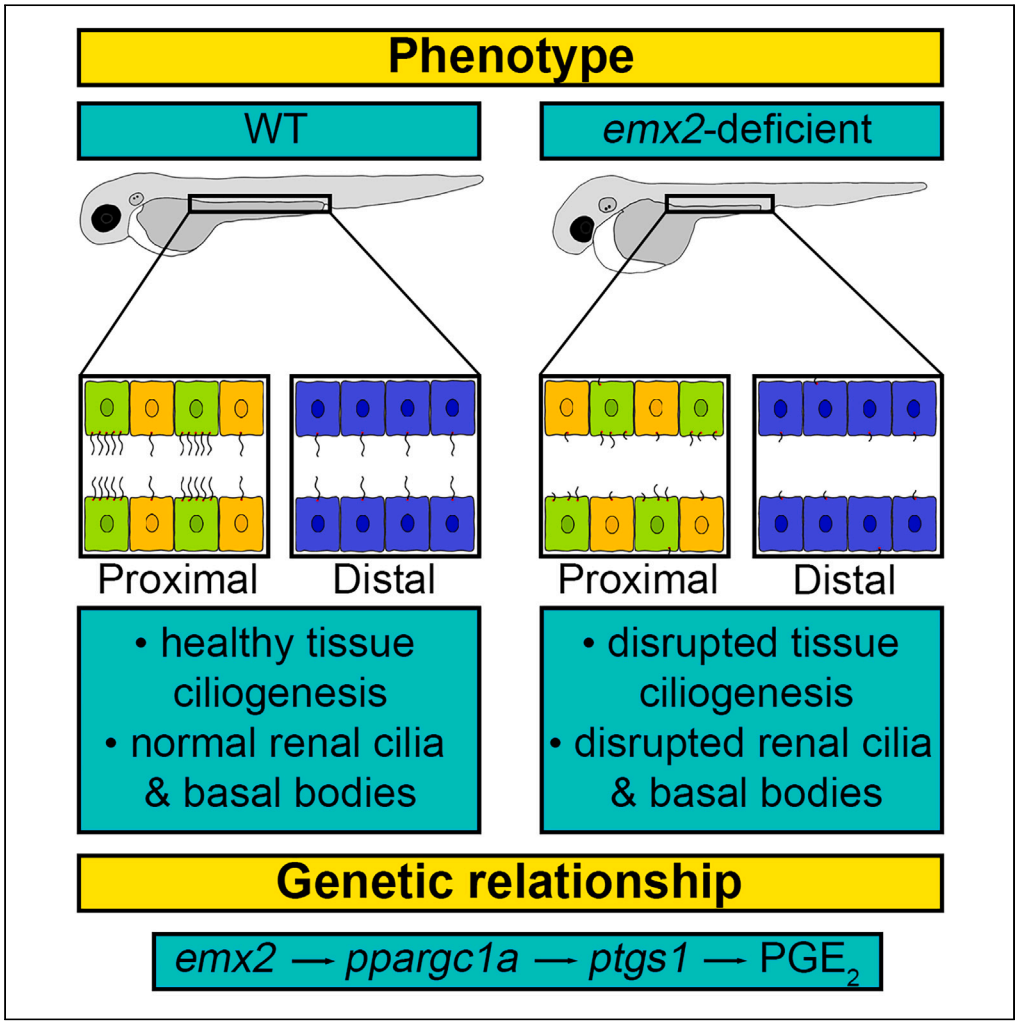

Thanh Khoa Nguyen, John-Michael Rodriguez, Hannah M. Wesselman, Rebecca A. Wingert

knguyen8@nd.edu (T.K.N.)
rwingert@nd.edu (R.A.W.)

Highlights

emx2 directs ciliogenesis in the pronephros, ear, neuromasts, and Kupffer's vesicle

Renal ciliated cell fate choice is reliant on *emx2* during pronephros segmentation

emx2 regulates prostaglandin biosynthesis through *ppargc1a* and *ptgs1*

Nguyen et al., iScience 27, 111271
December 20, 2024 © 2024 The Authors. Published by Elsevier Inc.
https://doi.org/10.1016/j.isci.2024.111271

iScience

CellPress
OPEN ACCESS

Article

Emx2 is an essential regulator of ciliated cell development across embryonic tissues

Thanh Khoa Nguyen,[1,*] John-Michael Rodriguez,[1] Hannah M. Wesselman,[1] and Rebecca A. Wingert[1,2,*]

SUMMARY

Cilia are hair-like organelles with vital physiological roles, and ciliogenesis defects underlie a range of severe congenital malformations and human diseases. Here, we report that *empty spiracles homeobox 2 (emx2)* is essential for cilia development across multiple embryonic tissues including the ear, neuromasts and Kupffer's vesicle (KV), which establishes left/right axial pattern. *emx2* deficient embryos manifest altered fluid homeostasis and kidney defects including decreased multiciliated cells (MCCs), determining that *emx2* is essential to properly establish several renal lineages. Further, *emx2* deficiency disrupted renal monociliated cells, MCCs and led to aberrant basal body positioning. We reported that *emx2* regulates prostaglandin biosynthesis in ciliogenesis and renal fate changes through key factors including *ppargc1a, ptgs1* and PGE_2. Our findings reveal essential roles of *emx2* in tissue cilia development, and identify *emx2* as a critical regulator of prostaglandin biosynthesis during renal development and ciliogenesis, providing insights relevant for future treatments of ciliopathies.

INTRODUCTION

Cilia are exquisite organelles that play crucial roles in ontogeny and physiology. Many vertebrate cells form a single cilium, while others form bundles of cilia and are termed multiciliated cells (MCCs). Proper ciliogenesis and ciliated cell fate choice are essential for diverse events ranging from body pattern formation to organ development, and defects in ciliated cell formation have catastrophic outcomes ranging from *situs inversus* to central nervous system disorders, retinopathies, liver and kidney diseases, among others.[1] As such, continuing to elucidate the mechanisms that control ciliogenesis and ciliated cell type specification has broad reaching significance and medical relevance.

empty spiracles homeobox 2 (*emx2/Emx2/EMX2)* is a homeodomain transcription factor homologous to the empty spiracles *(ems)* gene in *Drosophila,* which is crucial for head development.[2,3] In vertebrates, *emx2/Emx2/EMX2* is expressed during neuronal, auditory, olfactory and renal development.[4–17] Consistent with these sites of expression, previous studies uncovered a variety of phenotypes across tissues in animal models and humans deficient in *emx2/Emx2/EMX2*. For example, murine knockout of *Emx2* resulted in the disappearance of the kidney, ureters, gonads and genital tracts, and a lack of the Müllerian ducts.[7,18] *Emx2* murine knockouts also display central nervous system defects such as in hippocampus development.[9,18,19] In humans, *EMX2* mutations have been associated with schizencephaly, a rare brain disorder.[20–23] Recently, single cell RNA-seq data from patients with autism spectrum disorders revealed disrupted expression of *EMX2*,[24] and patients with Mayer-Rokitansky-Küster-Hauser (MRKH), a rare syndrome involving the malformation of Müllerian structures, have multiple variations in EMX2 sequence.[25] Most relevant to the present report, *emx2* deficiency has been linked to the disrupted formation of several ciliated cell types. Specifically, *emx2/Emx2* is needed to establish planar cell polarity in mechanosensory hair cells located in the auditory and lateral line systems of zebrafish and mammals. In these hair cells, Emx2/EMX2 is requisite to properly position the basal body, from which the kinocilium will form during sensory cell differentiation, and alterations of this placement change the orientation of the stereociliary bundle.[15,17,26–28] However, comparatively little is known about the role of *emx2* in the many other ciliated cell populations of the vertebrate embryo.

Here, we reported the essential role of *emx2* in several ciliated organs. Using the zebrafish model, we detected the presence of *emx2* transcripts across developing ciliated cells and found that *emx2* deficiency disrupted cilia formation in the Kupffer's Vesicle (KV), macula, neuromasts and the kidney. Further, *emx2* loss of function led to abnormal renal fluid flow and reductions in kidney MCC and distal late (DL) cell lineages—together, a suite of hallmarks that characterize developmental defects in prostaglandin signaling.[29–31] Indeed, we found that *emx2* deficiency significantly reduced expression of key prostanoid biosynthesis regulators: the Ppargc1a transcription factor, encoded by *peroxisome proliferator-activated receptor gamma, coactivator 1 alpha (ppargc1a),* and the Ptgs1 cyclooxygenase enzyme, encoded by *prostaglandin-endoperoxide synthase 1* (*ptgs1*). Renal ciliated cell development was rescued in *emx2* deficient animals by provision of *ppargc1a* transcripts, *ptgs1* transcripts or exogenous treatment with the prostanoid prostaglandin E_2 (PGE_2). Interestingly, we also found that *emx2* deficiency led to aberrant basal body positioning in the kidney, echoing previous findings on the role of *emx2* in sensory cell polarity. Finally,

[1]Department of Biological Sciences, Center for Stem Cells and Regenerative Medicine, Center for Zebrafish Research, Boler-Parseghian Center for Rare and Neglected Diseases, Warren Center for Drug Discovery, University of Notre Dame, Notre Dame, IN 46556, USA
[2]Lead contact
*Correspondence: knguyen8@nd.edu (T.K.N.), rwingert@nd.edu (R.A.W.)
https://doi.org/10.1016/j.isci.2024.111271

This is an open access article under the CC BY-NC license (http://creativecommons.org/licenses/by-nc/4.0/).

PGE_2 treatment rescued ciliogenesis in the KV of *emx2* deficient embryos and led to normal left/right axis formation, indicating that ciliary function was sufficiently restored to drive early patterning events—highlighting that prostaglandin signaling is vital to mediate ciliogenesis in non-renal cell types. In sum, our study has elucidated essential roles of *emx2* in ciliated cell development across multiple zebrafish embryonic tissues, and concluded that Emx2 influences prostaglandin biosynthesis to control renal and non-renal ciliated cell development.

RESULTS

Empty spiracles homeobox 2 is essential for ciliated cell development across multiple zebrafish embryonic organs

Previous studies have linked *emx2/Emx2/EMX2* expression to developing ciliated tissues in several species. In the zebrafish, *emx2* has been reported to be expressed in the proximal region of the zebrafish embryonic kidney, known as the pronephros.[12] To further study where *emx2* is expressed in the zebrafish embryo, we performed whole mount *in situ* hybridization (WISH) in wild-type (WT) 28 somite stage (ss) embryos. Interestingly, we found *emx2* expression in several locations that contain ciliated cells, including the pronephros, otic vesicle, and nasal placode (Figure 1A). In the zebrafish kidney, there are two types of ciliated epithelia within the nephron functional units: monociliated cells and MCCs.[32,33] The populations of monociliated tubule cells in the zebrafish kidney are patterned into discrete functional segments known as the proximal convoluted tubule (PCT), proximal straight tubule (PST), distal early (DE) and distal late (DL) at the 28 ss. Each of these segments is uniquely regulated by diverse nephrogenesis genes (Figure S1A).[34–36] At this time, MCCs are located from the PCT to the DE in a "salt and pepper" fashion amongst the monociliated cells (Figure S1A).[37–39] Within the pronephros, we noted that *emx2* transcripts were quite abundant within the region occupied by MCCs (Figure 1A). Therefore, we utilized double WISH using the MCC marker *odf3b* to assess whether MCCs or their neighboring epithelia expressed *emx2*. Interestingly, *emx2* transcripts colocalized with *odf3b*$^+$ cells by the 28 ss (Figure 1B). Furthermore, *emx2* transcripts were detected in the intercalated pronephric cells that were *odf3b*$^-$ at the 28 ss, thus indicating that the neighboring monociliated cells also expressed *emx2* (Figure 1B). Additionally, *emx2* transcripts colocalized with MCC progenitor markers *pax2a* and *jag2b* by the 24 ss, with *emx2* transcripts detected in both *pax2a*$^+$ cells and *jag2b*$^+$ cells. (Figure S1G). We also detected the presence of *emx2* transcripts within the bilateral stripes of renal progenitors that give rise to monociliated and MCC progenitors from 5 ss to the 17 ss (Figure S1C). Additionally, we observed *emx2* expression in the KV, a ciliated transient embryonic organ which initiates the left/right (L/R) pattern formation of organs such as the heart, thus has been likened to the mammalian node (Figure S1C).[40,41] Taken together, the expression of *emx2* in several ciliated organs suggested that *emx2* potentially plays a significant role in cilia development across zebrafish embryonic tissues.

To investigate the hypothesis that *emx2* is involved broadly in ciliogenesis, we examined cilia formation across tissues using the *emx2*$^{el586/el586}$ mutant line, referred to subsequently here as *emx2*$^{-/-}$, which encodes a 10 base pair deletion that induces a frameshift after amino acid 74 (of 247) (Figures S1B, S1E and S1F).[42] We performed whole mount immunofluorescence (IF) to detect acetylated α-tubulin, which marks cilia. Compared to WT embryo controls, *emx2*$^{-/-}$ mutants displayed dramatic reductions in cilia formation within the proximal pronephros segment occupied by MCCs (Figure 1C), as well as in distal segment regions where only monociliated cells are formed (Figure S1D). Next, we utilized whole mount IF to examine the KV organ during somitogenesis. At the 10 ss, *emx2*$^{-/-}$ mutants exhibited reduced cilia length in the KV compared to WT embryos (Figures 1D, 1E and Table S1). Next, using whole mount IF at 4 days post fertilization (dpf), we investigated ciliogenesis in the neuromasts, which are small epithelial receptor organs composed of sensory hair cells. Each sensory hair cell has a ciliary bundle composed of a single long kinocilium and many shorter stereocilia that sit to one side of the kinocilium. While WT embryos had normal neuromast structures with cilia bundled together, *emx2*$^{-/-}$ mutants occasionally displayed much shorter and disorganized neuromast cilia (Figure 1F). Quantification of cilia length in WT and *emx2*$^{-/-}$ revealed a statistically significant reduction in neuromast cell cilia length in the mutant embryos (Figures 1G and Table S1). Furthermore, *emx2*$^{-/-}$ mutants also displayed clear defects in otic vesicle development versus WT embryos at 4 dpf, including underdeveloped cilia in the posterior macula and crista (Figure 1H).

We next explored whether changes in ciliary function might be consequent to one of these overt morphological defects in cilia development. To do this, we investigated whether changes in L/R patterning, which is driven by the KV motile cilia, were associated with *emx2* deficiency by examining cardiac looping. We conducted WISH with WT and *emx2*$^{-/-}$ embryos at 55 hours postfertilization (hpf) using the cardiac marker *myl7*.[43] While all WT embryos displayed normal heart looping, some *emx2*$^{-/-}$ embryos experienced the randomization of heart looping, displaying *situs inversus* or *mid* phenotypes (Figures 1I, 1J and Table S1). Taken together, these studies indicate that *emx2* plays several vital roles in ciliated cell development across the zebrafish embryo which have not been previously appreciated.

Empty spiracles homeobox 2 deficiency causes phenotypes associated with renal cilia defects

Given the required roles of *emx2* in ciliated sensory cells,[15,17,26–28] and its co-expression with ciliated cells in the zebrafish pronephros, we next sought to further explore how loss of *emx2* function affects renal cilia development using several independent methods. In addition to the *emx2*$^{-/-}$ line, we developed an antisense knockdown model and an independent genetic model using CRISPR/Cas9. For the antisense strategy, we designed *emx2* splice blocking morpholino oligonucleotides (MOs) to target the splice donor and splice acceptor junctions between exon 1 and exon 2 (Figure S2A). Using RT-PCR and Sanger sequencing, we determined that the MOs resulted in the inclusion of intron 1, causing an in-frame stop codon, resulting in a truncated Emx2 protein (Figures S2B and S2C). For an independent mutant model, we generated F0 mosaic *emx2* crispants by multiplexing multiple sgRNAs targeting three distinct regions of exon 1 (Figure S3A). Crispant genotypes were confirmed using a T7 Endonuclease assay and Sanger sequencing (Figures S3B and S3C), and we found that the *emx2* sgRNA multiplex was >90% penetrant in inducing mosaicism (Figure S3D and Table S6).

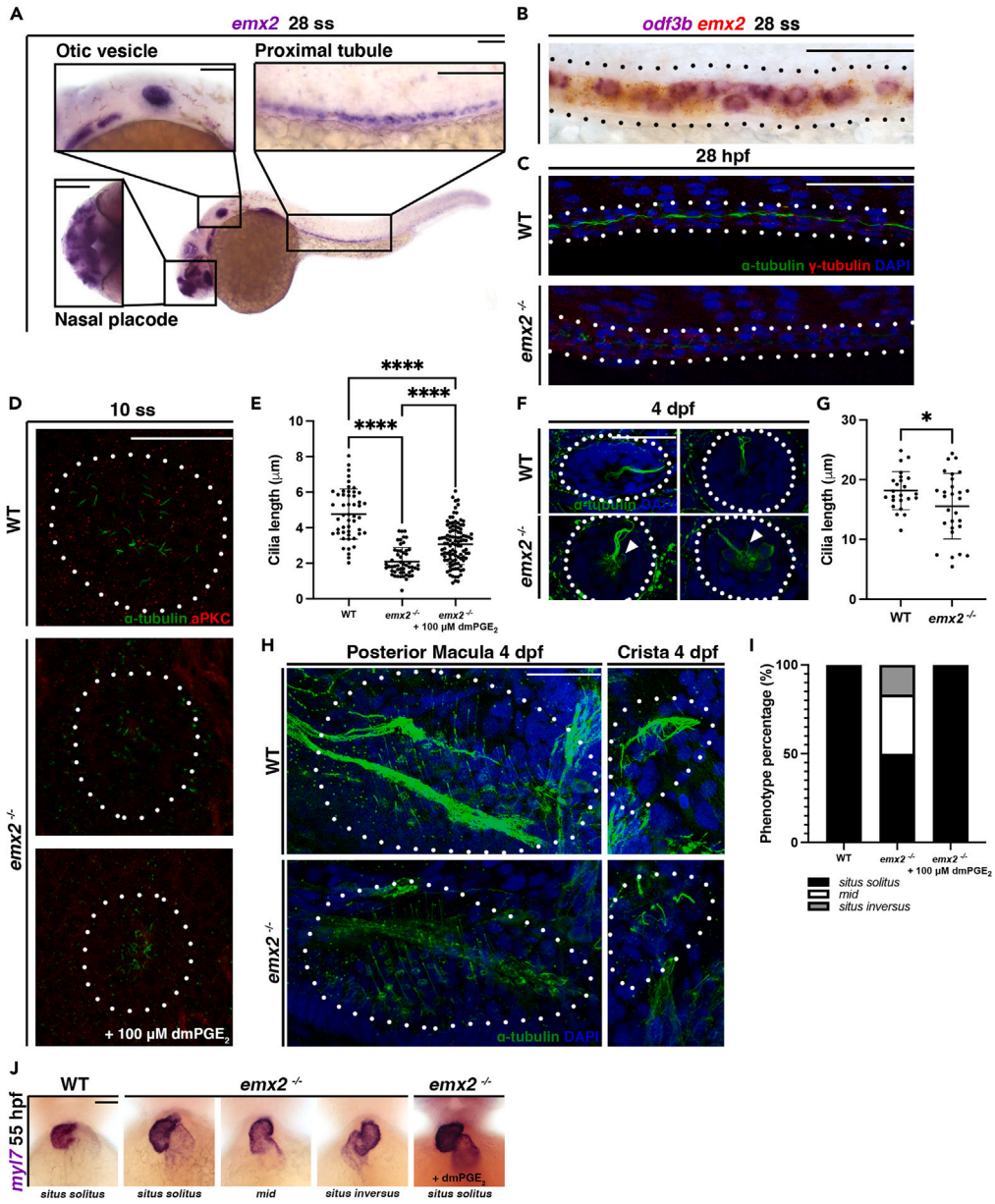

Figure 1. *emx2* is essential for cilia development in ciliated organs across the zebrafish embryo

(A) 28 ss WT embryo stained via WISH to illustrate *emx2* mRNA expression. Box is of approximate area of inset showing *emx2* expression in highly ciliated organs such as the otic vesicle, nasal placode and proximal tubule. Scale bar = 100 μm, otic vesicle and nasal placode inset = 50 μm, proximal tubule inset = 50 μm.

(B) 28 ss WT embryo stained via WISH for *emx2* and an MCC marker (*odf3b*). Scale bar = 50 μm.

(C) 28 hpf whole mount IF for acetylated α-tubulin (cilia, green), γ-tubulin (basal bodies, red), and DAPI (nucleus, blue) in the proximal pronephros of WT and $emx2^{-/-}$ embryos. Scale bar = 50 μm.

(D) 10 ss whole mount IF for acetylated α-tubulin (cilia, green) and anti-PKC (membrane boundary, red) in the KV of WT, $emx2^{-/-}$ embryos and $emx2^{-/-}$ embryos treated with $dmPGE_2$. Scale bar = 50 μm.

(E) KV cilia length between 10 ss WT, $emx2^{-/-}$ embryos and $emx2^{-/-}$ embryos treated with $dmPGE_2$.

(F) 4 dpf whole mount IF for acetylated α-tubulin (cilia, green) and DAPI (nucleus, blue) in the neuromast of WT and $emx2^{-/-}$ embryos. Scale bar = 25 μm.

(G) Neuromast cilia length between 4 dpf WT and $emx2^{-/-}$ embryos.

(H) 4 dpf whole mount IF for acetylated α-tubulin (cilia, green) and DAPI (nucleus, blue) in the posterior macula and crista of WT and $emx2^{-/-}$ embryos. Scale bar = 25 μm.

(I) Phenotype percentage of heart looping phenotypes between WT, $emx2^{-/-}$ embryos and $emx2^{-/-}$ embryos supplemented with $dmPGE_2$.

(J) 55 hpf WT, $emx2^{-/-}$ embryos and $emx2^{-/-}$ embryos supplemented with $dmPGE_2$ stained via WISH using heart marker *myl7*. Scale bar = 50 μm. Data presented on graphs are represented as mean ± SD; *$p < 0.05$, **$p < 0.01$ ***$p < 0.001$ and ****$p < 0.0001$ (t-test or ANOVA).

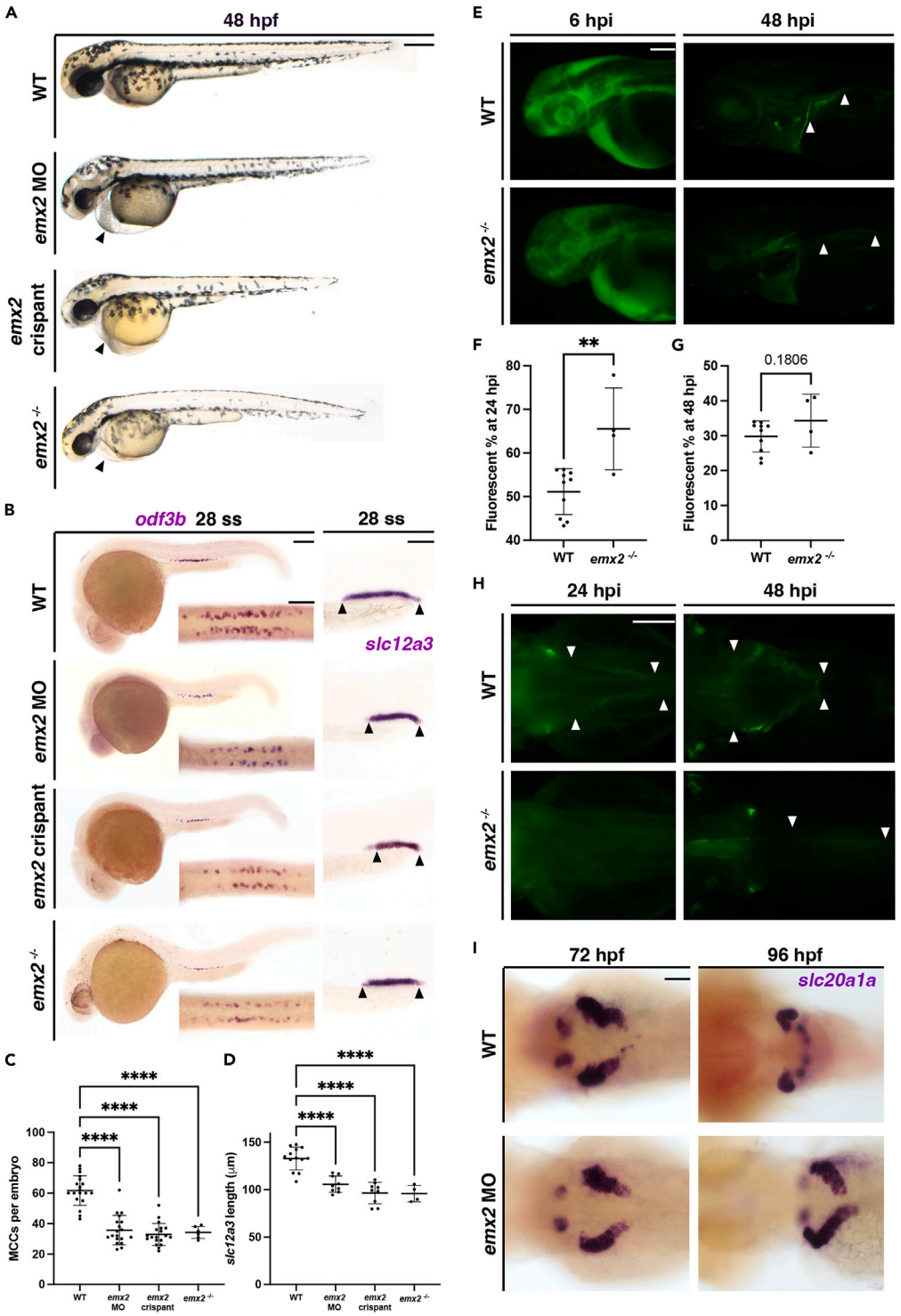

Figure 2. Loss of *emx2* causes phenotypes associated with cilia defects in the zebrafish pronephros

(A) WT, *emx2* MO, *emx2* crispant and *emx2*$^{-/-}$ embryos live imaging at 48 hpf. Arrows indicate pericardial edema. Scale bar = 200 μm.

(B) 28 ss WT, *emx2* MO, *emx2* crispant and *emx2*$^{-/-}$ embryos stained via WISH using the MCC marker *odf3b* and the DL marker *slc12a3*. Scale bars = 100 μm, DL and MCC inset = 50 μm.

(C) Number of MCCs per embryo between 28 ss WT, *emx2* MO, *emx2* crispant and *emx2*$^{-/-}$ embryos.

(D) *slc12a3* length between 28 ss WT, *emx2* MO, *emx2* crispant and *emx2*$^{-/-}$ embryos.

Figure 2. *Continued*

(E) Lateral view of WT and *emx2*$^{-/-}$ embryos at 6 hpi and 48 hpi after dextran-FITC injection. Arrows indicate fluorescent conjugate uptake. Scale bars = 100 μm.
(F) Percentage of remaining fluorescent at 24 hpi and (G) percentage at 48 hpi as compared to 6 hpi between WT and *emx2*$^{-/-}$ embryos.
(H) Dorsal view of WT and *emx2*$^{-/-}$ embryos at 24 hpi and 48 hpi after dextran-FITC injection. Arrows indicate fluorescent conjugate uptake. Scale bars = 100 μm.
(I) 72 hpf and 96 hpf WT and *emx2* MO stained via WISH for *slc20a1a* to mark PCT. Scale bar = 50 μm. Data presented on graphs are represented as mean ± SD; *$p < 0.05$, **$p < 0.01$ ***$p < 0.001$ and ****$p < 0.0001$ (t-test or ANOVA).

This suite of *emx2* loss of function models were then used to further explore the renal phenotypes associated with *emx2* deficiency, beginning with live morphology studies. At 48 hpf, the *emx2* morphant, *emx2* crispant and *emx2*$^{-/-}$ embryos exhibited pericardial edema and hydrocephalus, indicative of impaired kidney function (Figure 2A). We hypothesized that these *emx2* deficient phenotypes could be due to the lack of fluid flow resulting from changes in pronephros development, such as alterations in MCC development which frequently lead to the reduction or abrogation of luminal flow.[29–31] To investigate this, we performed WISH analysis using the specific MCC marker *odf3b* in WT and *emx2* deficient embryos. *emx2* morphant, *emx2* crispant and *emx2*$^{-/-}$ embryos had decreased *odf3b*$^{+}$ cells per embryo compared to WT controls (Figures 2B, 2C and Table S2). Additionally, WISH analysis using the specific MCC marker *cetn4*, which, similar to *odf3b*, marks differentiating MCCs, revealed a statistically significant reduction in MCC number in *emx2* deficient embryos (Figures S4A–S4D and Table S7).

Next, we wondered if this decrease in MCCs was associated with changes in MCC specification. MCC fate choice from the renal progenitor state occurs during the 10–26 ss, where MCC progenitors can be discerned based on expression of the transcription factor encoded by *pax2a* and components of the Notch signaling pathway such as the ligand encoded by *jag2b*.[29,32,33] WISH analysis revealed a statistically significant reduction in the number of *pax2a*$^{+}$ and *jag2b*$^{+}$ cells in *emx2* deficient embryos compared to WT, respectively (Figures S4B, S4C, S4E, S4F and Table S7). These observations are consistent with a role for Emx2 in directing MCC fate choice.

Interestingly, using the marker *slc12a3*, we also found a significant decrease in the length of the DL segment in *emx2* deficient embryos compared to WT (Figures 2B–2D and Table S2). We also surveyed other nephron segments using WISH and found no difference between WT and *emx2* deficient embryos in the length of the PST segment based on expression of *trpm7* or the DE segment based on expression of *slc12a1* (Figures S5A–S5D and Table S8). In addition, to determine if the observed changes in nephron segments in the *emx2* deficient embryos were related to changes in embryo size, we performed several body measurements in WT and *emx2* deficient embryos. Neither the distance from the tip to tail, distance from yolk to cloaca, or length of the yolk extension differed between WT and *emx2* deficient embryos (Figures S5E–S5H and Table S5). Therefore, we concluded that the changes observed in DL and MCC numbers in *emx2* deficient embryos reflect direct roles of *emx2* in pronephros development as opposed to indirect consequences related to changes in the size of the embryo. These results led us to conclude that *emx2* is essential for renal lineage development in the zebrafish pronephros.

To further explore if the decreases in renal MCCs were functionally significant, we next assessed nephron clearance. We microinjected WT and *emx2*$^{-/-}$ embryos with 40 kDa Dextran-FITC at 48 hpf, then performed live imaging at 6 hours post injection (hpi), 24 hpi and 48 hpi. Interestingly, we observed a delay in net fluid clearance in *emx2*$^{-/-}$ embryos, as well as delayed coiling morphogenesis of the PCT segment at 24 hpi and 48 hpi (Figures 2E–2H and Table S2). As previous studies have shown that nephron fluid flow plays an important role in PCT morphogenesis and cell migration,[44] we performed WISH using the PCT marker *slc20a1a*. Similarly, we observed a delay in PCT coiling in *emx2* morphants compared to WT embryos at 72 hpf and 96 hpf (Figure 2I).

Empty spiracles homeobox 2 deficiency causes several body morphology defects

Defects in *emx2* are known to affect a plethora of tissues such as brain, ear hair cell development, kidney and reproductive tracts in mice and humans.[7,9,15,17–19,23,25] In addition, our WISH data demonstrated a broad range of tissues labeled with *emx2* transcripts. Therefore, we also hypothesized that *emx2* deficiency in zebrafish will also cause several body morphology defects. Indeed, we observed pleiotropic phenotypes in *emx2* deficient embryos in addition to previously shown phenotypes in kidney and other ciliated organs. For instance, Alcian blue staining at 96 hpf revealed a gaping jaw in *emx2* morphants compared to WT embryos. In contrast to WT embryos which formed five ceratobranchial (CB) bones, *emx2* morphant formed less CB bones (Figure S6A). WISH staining using fin bud progenitor marker *mecom* showed a decreased fin bud area in *emx2* morphant compared to WT embryos (Figures S6B, S6C and Table S9). *o*-Dianisidine staining for erythrocytes at 48 hpf revealed the presence of blood clots around the head, eyeball and decrease in blood accumulation below the yolk ball in *emx2* morphants compared to WT controls (Figure S6D). Furthermore, Acridine Orange staining at 24 hpf revealed increased cell death across the body in *emx2* morphant compared to WT embryos, such as the brain, somites and cloaca (Figures S6E–S6J and Table S9). Overall, these results indicate that *emx2* is involved in several physiological processes throughout the body, such as regulating cartilage and fin development, vasculature, brain, and kidney development, which are consistent with previous studies.

Empty spiracles homeobox 2 induces prostaglandin biosynthesis in renal cilia development

In the zebrafish embryo, decreased MCCs in conjunction with a reduced DL nephron segment are hallmark characteristics of renal cilia defects due to reduction in prostaglandin biosynthesis from alterations in the function of the transcription coactivator encoded by *ppargc1a*.[30] Interestingly, previous studies have shown that myoblasts overexpressed with EMX2 had a 7.64-fold increase in *ppargc1a* (PGC-1α in mammal) expression.[45] Given our observed phenotype with decreased DL length and MCC numbers in our *emx2* deficient embryos, we hypothesized that *emx2* is upstream of *ppargc1a* in regulating prostaglandin biosynthesis in renal cilia development. *ppargc1a* has recently been shown to regulate key players in prostaglandin biosynthesis. Importantly, deficiency of *ppargc1a* significantly reduces the quantity of *ptgs1* transcripts in the 24 hpf zebrafish embryo, where the addition of *ptgs1* transcripts is sufficient to rescue cilia phenotypes in these *ppargc1a* deficient

embryos.[30] Further, PGE_2 is a molecule derived from PGH_2, a prostaglandin precursor, and a major prostanoid detected in the zebrafish embryo.[46] PGE_2 is a product of biosynthesis reactions catalyzed by *ptgs1* and *ptgs2* (also known as COX1 and COX2 respectively) from arachidonic acid,[47] and addition of PGE_2 also restores cilia formation and renal MCC fate in *ppargc1a* deficient embryos.[30]

To study if *emx2* induces prostaglandin biosynthesis in renal cilia development, we surveyed the promoter region of zebrafish *ppargc1a* and *ptgs1* for consensus sites for Emx2. Using the previously reported Emx2 consensus binding site,[45] we found 3 sites with striking similarities to the reported consensus site located within 10 kb upstream and downstream of *ppargc1a* open reading frame (ORF) for both strands (Figure S7E). Similarly, we also found 4 sites within 10 kb upstream and downstream of the *ptgs1* ORF for both strands (Figure S7F). The prevalence of consensus sites suggested potential interaction between Emx2 and these target genes. To investigate, we conducted WISH for *ppargc1a* at 28 ss. We observed a reduced domain of *ppargc1a* expression in the *emx2* morphant pronephros compared to WT embryos, and expression was qualitatively diminished elsewhere as well, such as the somites (Figures 3A, 3B and Table S3). Additionally, we also observed a reduction of the *ppargc1a* pronephros domain in *emx2* morphant compared to WT embryos at earlier stages such as 15 ss or 20 ss (Figures S7A–S7D and Table S10). WISH studies also revealed a reduction in the pronephros domain of the cyclooxygenase enzyme *ptgs1* at 28 ss, which is a downstream target of *ppargc1a* (Figures 3D, 3E and Table S3). Furthermore, qRT-PCR analysis revealed a statistically significant reduction in *ppargc1a* and *ptgs1* transcripts in *emx2* morphant compared to WT embryos at 28 ss (Figures 3C–3F and Table S3). Next, we explored if *emx2* influences the production of the prostaglandin biomolecule prostaglandin E_2 (PGE_2). We used a commercially available ELISA assay to measure endogenous PGE_2 level between WT and *emx2* morphant embryos at 28 ss stage. There was no significant difference in the average amount of endogenous PGE_2 in *emx2* morphants compared to WT embryos (Figure S7G and Table S10). This was surprising given the marked regional expression changes of *ppargc1a* and *ptgs1* observed in *emx2* deficient embryos, and therefore we hypothesize that there are important regional differences in endogenous PGE_2 levels that affect the kidney which were not captured in the ELISA assay which relies on the entire embryo.

Given these observations, we sought to determine if the renal lineage defects in *emx2* deficient embryos could be rescued by *ppargc1a* transcripts, *ptgs1* transcripts or exogenous PGE_2 treatment. Due to the similarities of phenotype between *emx2* morphant and $emx2^{-/-}$ embryos, and to reduce the number of animals used, here we performed rescue studies using *emx2* morphants due to the simplicity of sample generation. Interestingly, the provision of *ppargc1a* transcripts partially rescued live phenotype at 48 hpf and MCC number in the *emx2* deficient embryos at the 28 ss (Figures 3G–3I and Table S3). Similarly, the provision of *ptgs1* transcripts partially rescued live phenotype at 48 hpf and MCC number in *emx2* deficient embryos (Figures 3G–3I and Table S3). Additionally, to interrogate the effect of PGE_2 in MCC development in *emx2* deficient embryos, we performed drug treatments in which we incubated *emx2* deficient embryos with $dmPGE_2$, a more stable form of PGE_2 that is amenable to chemical genetics, from 6 hpf until 24 hpf. *emx2* deficient embryos supplied with $dmPGE_2$ also had a moderately rescued live phenotype at 48 hpf and had partially rescued MCC numbers per embryo compared to embryos treated with vehicle alone (Figures 3G–3I and Table S3). Provision of *ppargc1a* transcripts, *ptgs1* transcripts and treatment with $dmPGE_2$ were all moderately penetrant in rescuing live phenotype (Figure S3D and Table S6). Altogether, these comprehensive results lead us to conclude that *emx2* promotes prostaglandin biosynthesis by controlling the expression of *ppargc1a, ptgs1* and ultimately affects local PGE_2 production in the developing zebrafish.

Deficiency of *empty spiracles homeobox 2* leads to abnormal cilia formation and growth in renal tubule

Based on our data that *emx2* deficiency causes reduction in the number of MCCs per embryo and poor renal clearance, we hypothesized that *emx2* deficiency leads to abnormal cilia formation and growth in the epithelial cells of the nephron tubule. Cilia consist of a basal body that functions as a tubulin organizing center where the cilium grows from; a transition zone with proteins that help anchor cilia and function as a gate for proteins to travel between ciliary compartments; and lastly, an axoneme that protrudes from the cell and is comprised of microtubules that are covered by the unique ciliary membrane and ciliary tip.[48–50] To interrogate this hypothesis, we performed whole mount IF to detect acetylated α-tubulin (cilia), γ-tubulin (basal bodies) and DAPI (nucleus) in WT, *emx2* morphant and $emx2^{-/-}$ embryos at the 28 hpf stage (Figure 4A and Figure S10A). We noticed that in the proximal pronephros, cilia length was significantly shorter in *emx2* morphant and $emx2^{-/-}$ embryos compared to WT controls (Figures 4B and Table S4). We also observed a decrease in proximal fluorescent intensity of acetylated α-tubulin in *emx2* morphant and $emx2^{-/-}$ embryos compared to WT embryos (Figures 4C and Table S4). Additionally, in the proximal pronephros, we observed a significant decrease in the percentage of ciliated basal bodies and the number of basal bodies and in both *emx2* morphant and $emx2^{-/-}$ embryos compared to WT (Figures 4D, 4E and Table S4). Consistent with our observation that *emx2* deficiency leads to decreased MCC formation, our data suggest there is abnormal cilia formation and growth in the pronephros proximal tubule. To investigate our ciliopathic phenotype further, we examined the distal tubule via IF (Figure S8A). Consistently, we also observed that cilia length in the distal tubule was significantly decreased in *emx2* morphant and $emx2^{-/-}$ embryos compared to WT (Figure S8B and Table S11). We also observed a decrease in the distal fluorescent intensity of acetylated α-tubulin in *emx2* morphant and $emx2^{-/-}$ embryos compared to WT embryos (Figure S8C and Table S11). Similarly, there was a decrease in percentage of ciliated basal bodies in *emx2* morphant and $emx2^{-/-}$ embryos compared to WT (Figure S8D and Table S11). *emx2* deficient embryos also exhibited fewer numbers of basal bodies compared to WT in the proximal pronephros (Figure 4E), and $emx2^{-/-}$ mutants, but not *emx2* morphants, had decreased basal bodies in the distal pronephros (Figure S8E and Table S11). Altogether, our data indicated that cilia formation is disrupted in both the proximal and distal domain in *emx2* deficient embryos, and support our conclusion that *emx2* is essential for renal ciliogenesis.

Empty spiracles homeobox 2 mediated ciliogenesis operates via prostaglandin biosynthesis factors

Since the overexpression of prostaglandin biosynthesis factors (*ppargc1a, ptgs1)* or $dmPGE_2$ treatment successfully rescued MCC formation in *emx2* morphants, next we hypothesized that the overexpression of prostaglandin biosynthesis factors would also rescue ciliogenesis within

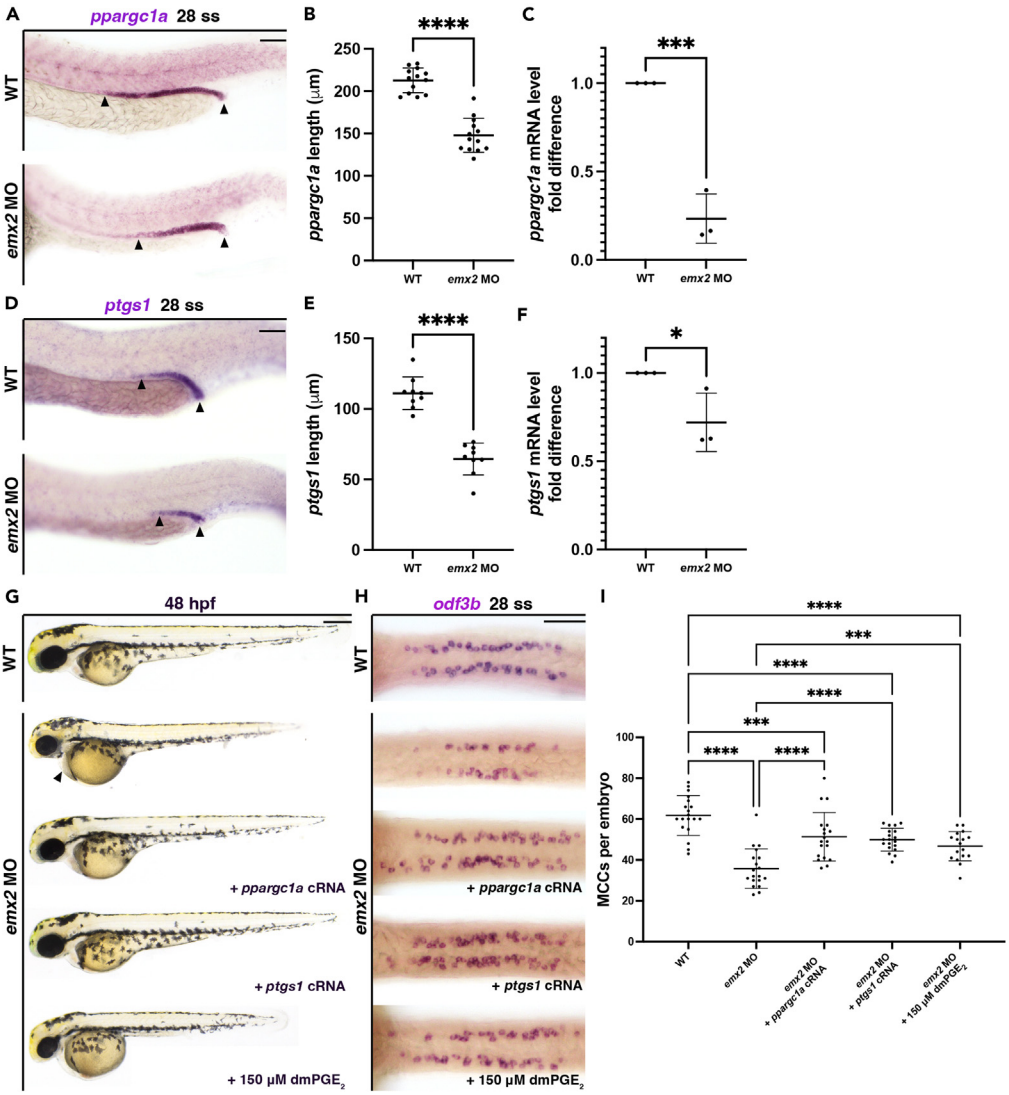

Figure 3. *emx2* induces prostaglandin biosynthesis in renal cilia development

(A) 28 ss WT and *emx2* MO embryos stained via WISH for *ppargc1a*. Scale bar = 50 μm.

(B) *ppargc1a* length between 28 ss WT and *emx2* MO embryos.

(C) Relative *ppargc1a* mRNA expression between WT and *emx2* MO embryos.

(D) 28 ss WT and *emx2* MO embryos stained via WISH for *ptgs1*. Scale bar = 50 μm.

(E) *ptgs1* length between 28 ss WT and *emx2* MO embryos.

(F) Relative *ptgs1* mRNA expression in WT and *emx2* MO embryos.

(G) Live imaging for different treatment groups at 48 hpf. Arrow indicates pericardial edema. Scale bar = 200 μm.

(H) 28 ss embryos stained via WISH for MCC marker *odf3b* for different treatment groups. Scale bar = 50 μm.

(I) Number of MCCs per embryo between different treatment groups at 28 ss. Data presented on graphs are represented as mean ± SD; *$p < 0.05$, **$p < 0.01$ ***$p < 0.001$ and ****$p < 0.0001$ (t-test or ANOVA).

emx2 morphants. Indeed, provision of *ppargc1a* transcripts to *emx2* deficient embryos rescued cilia length, acetylated α-tubulin intensity and percentage of ciliated basal bodies in both the proximal and distal domain of the pronephros (Figures 4A–4D, S8A–S8D and Table S4). Similarly, provision of *ptgs1* transcripts to *emx2* deficient embryos restored ciliogenesis throughout the nephron tubules, as did incubation with exogenous $dmPGE_2$ (Figures 4A–4D, S8A–S8D and Table S4).

To interrogate if there is any gain of function effect, we performed whole mount IF to detect acetylated α-tubulin (cilia), γ-tubulin (basal bodies) and DAPI (nucleus) in WT, WT provided with *ppargc1a* transcripts and WT provided with *ptgs1* transcripts at the 28 hpf stage (Figures S9A and S9B). We observed non-significant differences in proximal cilia length, percentage of ciliated basal bodies and number of basal bodies (Figures S9C–S9E and Table S12). Similarly, we observed non-significant differences in distal cilia length, percentage of

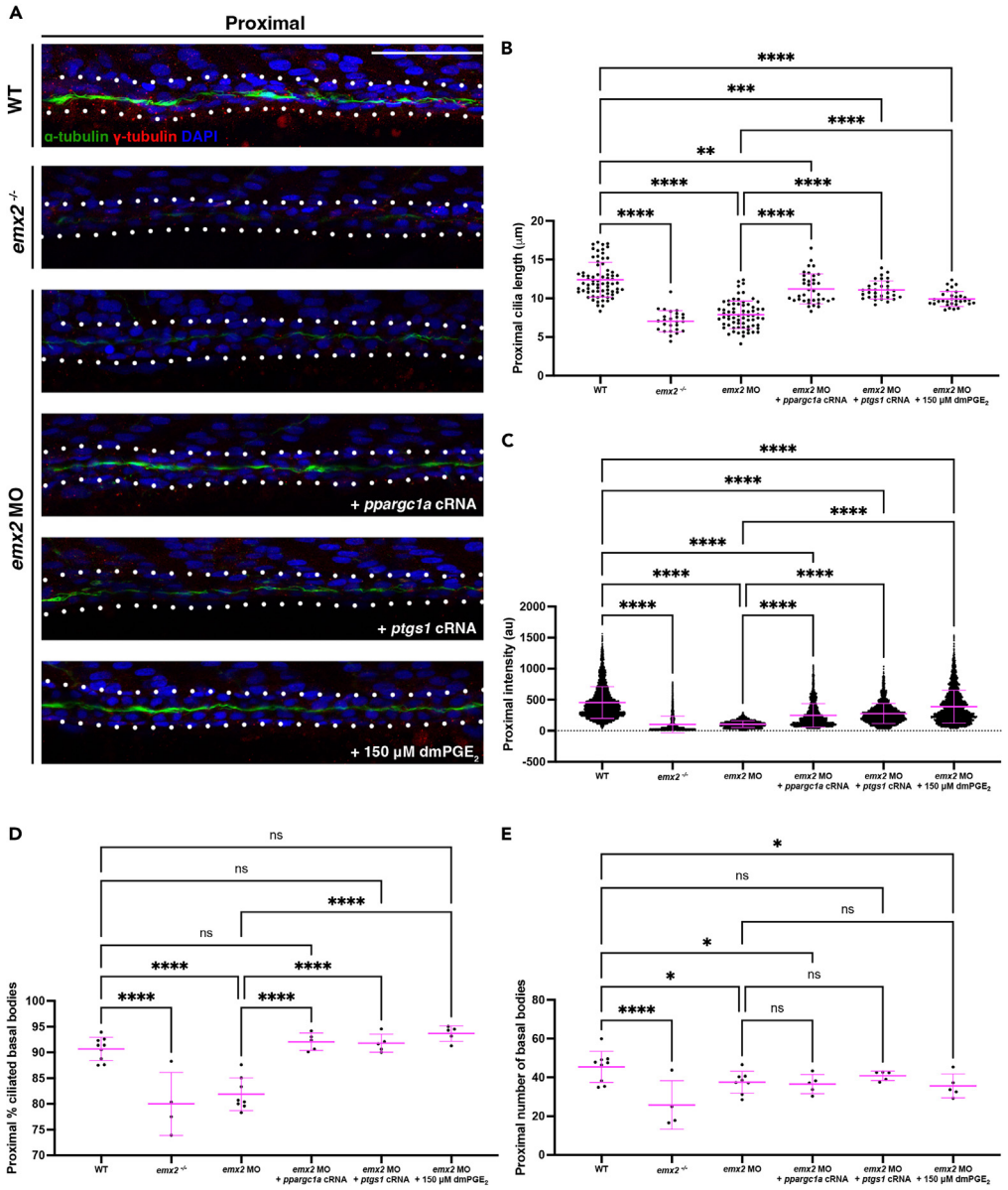

Figure 4. Cilia loss in proximal pronephros due to *emx2* deficiency can be rescued by supplement of key factors in prostaglandin biosynthesis

(A) 28 hpf whole mount IF for acetylated α-tubulin (cilia, green), γ-tubulin (basal bodies, red), and DAPI (nucleus, blue) in the proximal pronephros between different treatment groups. Scale bar = 50 μm.

(B) Cilia length for the proximal pronephros between different treatment groups.

(C) Fluorescence intensity plot of α-tubulin intensity in the proximal pronephros between different treatment groups.

(D) Percentage of ciliated basal bodies/total basal bodies in the proximal pronephros between different treatment groups.

(E) Number of basal bodies in the proximal pronephros between different treatment groups. Data presented on graphs are represented as mean ± SD; *$p < 0.05$, **$p < 0.01$ ***$p < 0.001$ and ****$p < 0.0001$ (t-test or ANOVA).

ciliated basal bodies and number of basal bodies (Figures S9F–S9H and Table S12). Additionally, a previous study also found no significant gain-of-function effect between WT and WT treated with $dmPGE_2$.[30] Therefore, we concluded that there is no significant gain-of-function phenotype. Interestingly, *ppargc1a* transcripts, *ptgs1* transcripts or $dmPGE_2$ had no effect on the number of proximal or distal basal bodies in *emx2* morphants (Figures 4E, S8E and Table S4). From this, we hypothesize that *emx2* has an essential role in basal body formation that does not operate through prostaglandin signaling. Collectively, these results enable us to discern that the ciliary growth defects in the pronephros from *emx2* loss of function resulted from disruptions in PGE_2 biosynthesis, specifically establishing that *emx2* regulates the Ppargc1a/Ptgs1/PGE_2 signaling cascade to control renal ciliogenesis.

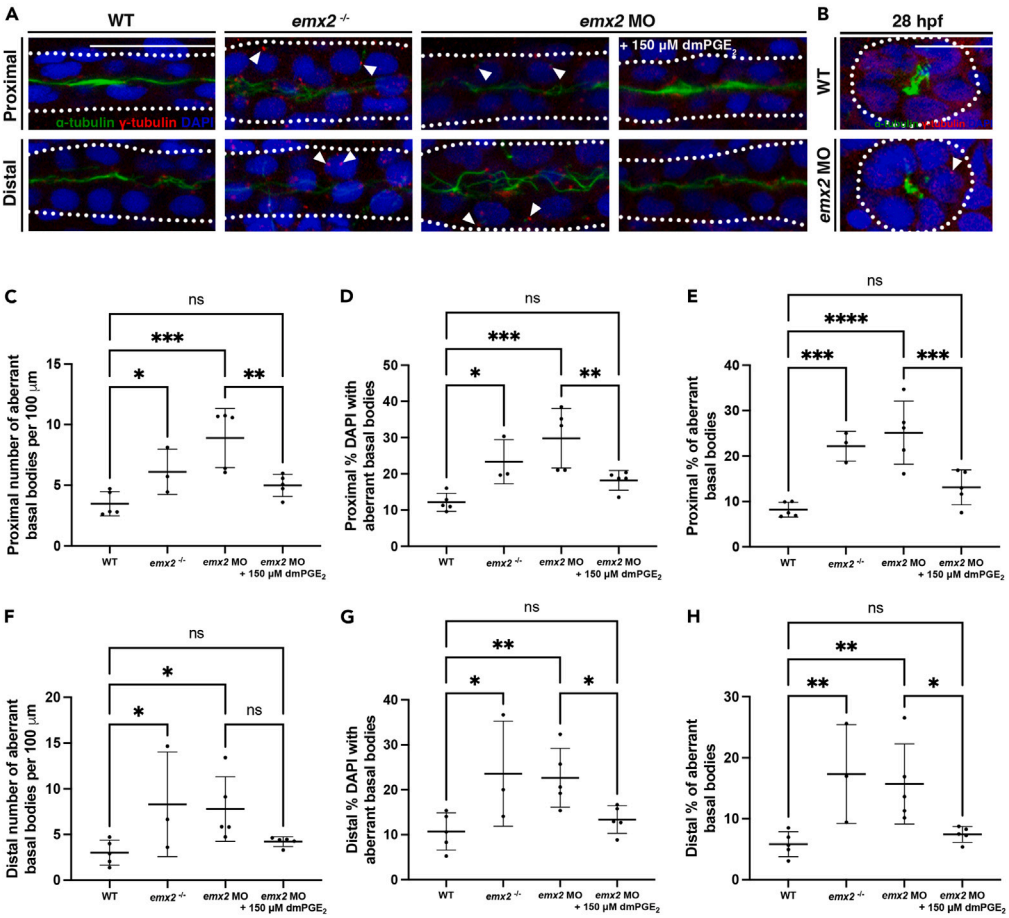

Figure 5. Basal body aberrancy in pronephric tubule due to *emx2* deficiency can be rescued by prostaglandin

(A) 28 hpf whole mount IF for acetylated α-tubulin (cilia, green), γ-tubulin (basal bodies, red), and DAPI (nucleus, blue) in the proximal and distal pronephros between different treatment groups. Arrows indicate aberrant basal bodies. Scale bar = 50 μm.

(B) 28 hpf whole mount IF for acetylated α-tubulin (cilia, green), γ-tubulin (basal bodies, red), and DAPI (nucleus, blue) in the sectioned pronephric tubule between WT and *emx2* MO. Arrow indicates an aberrant basal body. Scale bar = 12.5 μm.

(C) Proximal number of aberrant basal bodies per 100 μm between different treatment groups.

(D) Proximal percentage of DAPI cells that make up the pronephric tubule with aberrant basal bodies between different treatment groups.

(E) Proximal percentage of aberrant basal bodies between different treatment groups.

(F) Distal number of aberrant basal bodies per 100 μm between different treatment groups.

(G) Distal percentage of DAPI cells that make up the pronephric tubule with aberrant basal bodies between different treatment groups.

(H) Distal percentage of aberrant basal bodies between different treatment groups. Data presented on graphs are represented as mean ± SD; *$p < 0.05$, **$p < 0.01$ ***$p < 0.001$ and ****$p < 0.0001$ (t-test or ANOVA).

Empty spiracles homeobox 2 regulates basal body development in renal cilia

The basal body is an important structure of the cilium. The basal body is made up of a centriole, which is the locus where cilia growth happens.[51,52] After the centriole is generated, basal bodies migrate and fuse with the apical surface of the cell. Basal body docking, thus, is an important and essential phenomenon for proper cilia development. Previous studies on *emx2* have demonstrated a significant role of Emx2 in controlling hair bundle polarity reversal in sensory hair cells in the ear hair cells and neuromasts, especially in positioning the basal body from which the sensory cilia grow from.[15,17,26–28] However, there has not been much known about the role of *emx2* in basal body positioning in renal cilia. Due to the implicated role of *emx2* in basal body positioning, we hypothesized that *emx2* deficient embryos may have aberrant basal bodies compared to WTs.

To investigate basal body positioning in zebrafish renal cilia, we performed whole mount IF to detect acetylated α-tubulin (cilia), γ-tubulin (basal bodies) and DAPI (nucleus) in WT and *emx2* deficient embryos at the 28 hpf stage (Figure 5A). We examined whether cells that make up the pronephric tubule possessed basal bodies lacking proper apical orientation. Interestingly, we identified basal bodies with non-apical orientation in the proximal tubule in *emx2*$^{-/-}$ and *emx2* morphant embryos compared to WT embryos (Figure 5A). To further investigate, we performed whole mount IF to detect acetylated α-tubulin (cilia), γ-tubulin (basal bodies) and DAPI (nucleus) in the

sectioned pronephric tubule of WT and *emx2* deficient embryos at the 28 hpf stage (Figure 5B). To our surprise, we also detected basal bodies with non-apical orientation having little to no cilia development in *emx2* deficient embryos (Figure 5B). To quantify this, we scored each of those basal bodies as an aberrant basal body. There was a statistically significant increase in the incident of aberrant basal bodies per 100 μm in the proximal tubule in both *emx2* deficient groups compared to WT (Figures 5C and Table S5). Next, we found that there was an increase in the percentage of individual cells that make up the proximal tubule with aberrant basal bodies in both *emx2* deficient groups compared to WT (Figures 5D and Table S5). We also found an increase in the overall percentage of aberrant basal bodies in the proximal tubule in both *emx2* deficient groups compared to WT (Figures 5E and Table S5). We also surveyed the distal tubule for aberrant basal bodies. Similar to the proximal tubule, there was an increased incidence of basal bodies with non-apical orientation in $emx2^{-/-}$ and *emx2* morphant embryos compared to WT embryos (Figure 5A). Interestingly, in both proximal and distal tubule, we observed misplaced basal bodies often with stunted cilia projections (Figure 5A). Similar to the proximal tubule, we observed an increase in the incident of aberrant basal bodies per 100 μm in the distal tubule in both *emx2* deficient groups compared to WT (Figures 5F and Table S5). Additionally, we observed an increase in the percentage of DAPI cells that make up the distal tubule with aberrant basal bodies in both *emx2* deficient groups compared to WT (Figures 5G and Table S5), and an increase in the percentage of aberrant basal bodies in the distal tubule in both *emx2* deficient groups compared to WT (Figures 5H and Table S5). Our data show that the deficiency of *emx2* leads to incorrect basal body location in both the proximal and distal renal tubule cells. Thus, *emx2* serves an important role in basal body positioning within the zebrafish pronephros.

As our data have shown that treatment with $dmPGE_2$ successfully rescued MCC formation in *emx2* morphants, we were next interested in whether $dmPGE_2$ treatment can rescue our aberrant basal body phenotypes in *emx2* deficient embryos. To do so, we injected *emx2* MO at 1-cell stage, and performed drug treatment with injected embryos with $dmPGE_2$ starting from 6 hpf until 28 hpf. Next, we performed whole mount IF to detect acetylated α-tubulin (cilia), γ-tubulin (basal bodies) and DAPI (nucleus) at 28 hpf stage (Figure 5A). Interestingly, in the proximal tubule, we saw a rescue in the number or aberrant basal bodies per 100 μm, percentage of cells with aberrant basal bodies, and percentage of aberrant basal bodies in *emx2* morphants supplemented with $dmPGE_2$ compared to *emx2* morphants alone (Figures 5C–5E and Table S5). Similarly, in the distal tubule, we saw a rescue in the number of aberrant basal bodies per 100 μm, percentage of cells with aberrant basal bodies, and percentage of aberrant basal bodies in *emx2* morphants supplemented with $dmPGE_2$ compared to vehicle (Figures 5F–5H and Table S5). Together, these data indicate that PGE_2 is sufficient to rescue defective basal body positioning in *emx2* deficient embryos. We concluded that *emx2* mediates prostaglandin signaling to control basal body positioning in the zebrafish pronephros.

Modulation of prostaglandin E_2 level restores ciliogenesis defects in the Kupffer's vesicle and rescues heart looping

Finally, we were curious to explore whether prostaglandin signaling was a component of the ciliogenesis defect in other cell types of *emx2* deficient embryos. To examine this, we performed drug treatments in which we supplied $emx2^{-/-}$ embryos with $dmPGE_2$ from 6 hpf until 10 ss. Interestingly, we found that $emx2^{-/-}$ embryos supplied with $dmPGE_2$ exhibited a statistically significant increase in cilia length in the KV (Figures 1E and Table S1). Furthermore, $dmPGE_2$ treated $emx2^{-/-}$ embryos underwent normal cardiac looping, with a complete restoration of the *situs solitus* phenotype at 55 hpf (Figures 1I, 1J and Table S1). We hypothesize that an optimal level of prostaglandin signaling is necessary to support ciliary function in the KV, and thereby establish normal heart randomization. These results suggest that Emx2 regulates the prostaglandin molecule PGE_2 in controlling heart randomization, suggesting a role of Emx2 in controlling L/R patterning through prostaglandin signaling, and may have implications for the development other non-renal ciliated cells during embryogenesis.

DISCUSSION

Knowledge about the molecular mechanisms governing ciliated cell development is critical for understanding organogenesis, as well as addressing a broad spectrum of birth defects and diseases that emerge from ciliary dysfunction. The present work identifies the Emx2 transcription factor as essential for cilia formation across multiple organs and a director of ciliated cell fate choice during the process of kidney lineage establishment in zebrafish. Furthermore, we determined that Emx2 has a key role in regulating the recently identified Ppargc1a/Ptgs1 genetic pathway, which produces the prostanoid signaling molecule PGE_2 (Figure S1A). Specifically, our work has shown that the Emx2 mediated production of PGE_2 controls monociliated cell versus MCC fate choice during nephrogenesis in the embryonic zebrafish kidney, where it also drives normal ciliogenesis in these cell types, and that this pathway is relevant to ciliogenesis in the KV where defects lead to abnormal L/R patterning of the heart.

The Emx2/EMX2 transcription factor is well known for playing crucial roles during development, and there have been many fascinating discoveries about its roles in mechanosensory hair cell ontogeny. *Emx2* expression was first noted in olfactory placodes and later epithelium in mice, organs known to be highly ciliated,[5] and subsequent work revealed that Emx2 had a vital role in ear hair cell development, where mouse mutants formed 60% fewer auditory hair cells and exhibited the disruption of cochlear hair cell polarity, with polarity reversal across striola being damaged as well.[15] Conditional knockout of *Emx2* in hair cells has been found similarly to display lack of line of polarity reversal in the otolith.[53] Several landmark studies have elucidated the important role of *emx2/Emx2* in regulating hair cell orientation by regulated by core planar cell polarity in neuromasts[17,27,54] as well as mouse maculae.[55] Recent work has also revealed that EMX2 acts to polarize GPR156, a G-protein coupled receptor to signal through Gαi and trigger a 180° reversal in hair cell orientation.[56] However, the intriguing notion that Emx2 might possess functions in aspects of ciliated cell development in non-sensory cell types has not been explored until the present work.

Here, our work has shown that Emx2 is required for ciliogenesis across several tissues of the zebrafish. In the absence of Emx2, we found that shortened or disorganized cilia form in the KV, neuromasts, otic vesicle, and the pronephros. Further, basal body positioning is defective in pronephros tubule cells in *emx2* deficient embryos, recapitulating the role of Emx2 in sensory hair cells. Roles for EMX2 in the kidney have been a challenge to study because *Emx2* knockout mice die postnatally within a few hours and exhibit catastrophic organ abnormalities, prominently an absence of the kidneys and other parts of the urogenital system.[18,19] Thus, this has precluded the analysis of EMX2 function in cell fate specification or differentiation. However, here using the zebrafish, we have demonstrated that *emx2* controls components of renal cell fate decisions and differentiation within pronephric nephrons, and that both processes involve the Emx2 modulation of prostaglandin biosynthesis during early embryogenesis.

Prostaglandin biosynthesis has long been studied as an important physiological process controlling cilia development. A decade ago, it was found that PGE_2 is important for regulating anterograde intraflagellar transport in ciliogenesis.[57] Regulation of prostaglandin signaling has been recently identified as a potential treatment for the condition nephronophthisis (NPH), a rare renal ciliopathy. Using *Nphp1* KO mouse, a major gene important for primary cilium and cellular junctions, it was found that prostaglandin molecule PGE_1 and Taprenepag, a PGE_2 receptor agonist alleviated ciliopathy phenotypes in the *Nphp1* KO mouse.[58] This highlights the importance of understanding how prostaglandin signaling is regulated in the context of ciliogenesis. Here, by reporting the role of Emx2 as an essential inducer of prostaglandin biosynthesis during renal ciliogenesis, we address an important knowledge gap that is relevant to the treatment of ciliopathies.

Within MCC development, several studies have demonstrated that prostaglandin signaling is essential for renal ciliated cell development, where *ppargc1a* is requisite to control prostaglandin biosynthesis.[29,30] Interestingly, overexpression of EMX2 in cultured muscle cells led to their upregulation of PGC-1α (also known as *ppargc1a* in zebrafish).[45] Until now, however, the relationship between *emx2* and *ppargc1a* has not been explored during kidney development or ciliogenesis. Herein, our work has reported that *emx2* is upstream of *ppargc1a* and controls prostaglandin biosynthesis to modulate both ciliogenesis and the process of renal ciliated cell fate choice between that of a monociliated and MCC identity. MCCs are found in the zebrafish kidney, but only in the human fetal kidney[59] as well as in renal pathological conditions.[60–62] Therefore, knowledge of MCC development and what genes are responsible for MCC development has relevance for understanding the pathogenesis of numerous kidney diseases.

Future studies are needed to delineate the relationship of Emx2 with other genetic factors during kidney development. Interestingly, Emx1 has been suggested to compensate for Emx2 deficiency in the telencephalon.[19] Additionally, EMX1 and EMX2 expression have been found to overlap in the olfactory bulb and amygdaloid complex.[8] Given that *emx1* and *emx2* are paralogs of each other, and previous study has demonstrated the importance of *emx1* in nephron development in zebrafish,[63] it is possible that *emx2* also interacts with *emx1* in kidney tubule development. Previous studies have shown that Notch1a downregulates Emx2 expression in controlling hair cell polarity.[27,28] Interestingly, previous studies have shown that Notch signaling is important for restricting MCC formation.[64,65] Notch signaling has also been found to inhibit *etv5a*, a transcription factor essential for MCC development.[65] Therefore, there remains a question of how *emx2* interacts with Notch signaling in regulating MCC development in the zebrafish kidney.

Additionally, previous studies have shown a link between *Emx2* and WNT/β-catenin signaling in nephron development. qRT-PCR have demonstrated a decrease in *Emx2* and *Lim1* mRNA in β-catenin mutants when compared to WT. Additionally, β-catenin mutants also showed decreased expression of *Pax2*, *c-ret*, *Wnt11* and *Gdnf* compared to WT.[66] Notably, the knockdown of EMX2 has also been reported to promote canonical WNT signaling in lung cancer cells.[67] Furthermore, previous studies found that *Pax2* regulates *Emx2* in the Wolffian duct in mouse, and *Emx2* participates in a complex renal gene regulatory network, including *Pax2/8*, *Gata3* and *Lim1*.[68,69] Interestingly, most of these studies have been conducted in mouse models. Therefore, there remains open a question of whether mammalian *Emx2/EMX2* also participates in these physiological pathways as shown here in the zebrafish kidney. Notably, given our understanding of the role of *emx2* in controlling MCC development in zebrafish kidney via prostaglandin biosynthesis, it will be interesting to see how *emx2* and prostaglandin biosynthesis fit into this greater gene regulatory network in renal development.

Overall, the present study has further expanded our knowledge of Emx2 as an essential transcription factor across multiple developing organs. This work has reported that Emx2 modulates prostaglandin biosynthesis to control renal ciliogenesis and kidney cell fate decisions, and further, that Emx2 control of ciliogenesis in non-renal cell types can also involve modulating prostaglandin signaling. These findings have broad implications to understanding the mechanisms of ciliated cell development and the basis of ciliopathic conditions.

Limitations of study

There are a number of limitations in the present report that can be addressed through further research. First, while we identified *emx2* as a critical regulator of cilia development in zebrafish tissues, future studies are needed to elucidate whether *Emx2/EMX2* is necessary for ciliated cell development in mammalian tissues, including humans. As our study was conducted at an early embryonic stage in zebrafish, it remains to be determined whether *emx2* function is also relevant to cilia formation and maintenance in juvenile and adult vertebrates. Additionally, while we identified Emx2 consensus binding sites within both the *ppargc1a* and *ptgs1* ORFs, and thus can reasonably speculate that these sequences are functionally relevant, this putative direct regulatory interaction needs to be probed experimentally using chromatin immunoprecipitation sequencing (ChIP-Seq). Subsequent gene editing to modify the Emx2 binding sites and examine the consequence for *ppargc1a* and *ptgs1* gene expression would be important to further validate any direct interactions, and to determine the relative importance compared to other more distant regulatory sites. Finally, a recent study from our laboratory established that the transcription factor Esrrγa regulates fate choice and ciliogenesis in the nephron tubule by controlling prostaglandin synthesis—events

that similarly involve the genetic regulation of *ppargc1a* and *ptgs1*.[31] Therefore, it will be important to next discover the relationship between Emx2 and Esrrγa in controlling renal ciliated cell ontogeny.

RESOURCE AVAILABILITY

Lead contact

Further information and requests for resources and reagents should be directed to and will be fulfilled by the lead contact, Rebecca A. Wingert (rwingert@nd.edu).

Materials availability

The study did not generate any unique reagents. The *emx2*$^{el586/el586}$ mutant line was provided by Dr. Lindsey Barske (Cincinnati Children's Hospital, Ohio).

Data and code availability

- Data: This study did not generate any unique dataset
- Code: This study did not generate any original code
- Additional information: All used software is listed in key resources table. Any additional information from this article is available upon request from the lead contact.

ACKNOWLEDGMENTS

We thank the staff of the Department of Biological Sciences for support and the Center for Zebrafish Research at the University of Notre Dame for exceptional care of our zebrafish system. We are grateful for the members of Wingert Lab for assistance with this work. This work was supported by funds to R.A.W. from the College of Science and the generosity of the Gallagher Family for their support of stem cell research. We thank the Notre Dame Integrated Imaging Facility for providing us with the imaging facility that allowed us to take several images from this article, and especially Sara Cole for her incredible expertise and guidance. We would like to thank Dr. Lindsey Barske for generously providing us with the *emx2*$^{el586/el586}$ zebrafish line. T.K.N. would like to personally thank R.A.W., R.R., and P.B. for their incredible mentorship. R.A.W. dedicates this work to the love of S.B.C.W.

AUTHOR CONTRIBUTIONS

Conceptualization: T.K.N., H.M.W., and R.A.W.; methodology: T.K.N., and J.M.R.; investigation: T.K.N., J.M.R., and R.A.W.; resources: R.A.W.; writing: T.K.N. and R.A.W.; supervision and funding: R.A.W.

DECLARATION OF INTERESTS

The authors declare no competing interests.

STAR★METHODS

Detailed methods are provided in the online version of this paper and include the following:

- KEY RESOURCES TABLE
- EXPERIMENTAL MODEL AND STUDY PARTICIPANT DETAILS
- ANIMAL MODELS
- METHOD DETAILS
  - Whole mount *in situ* hybridization (WISH)
  - Dextran-FITC injections
  - Acridine Orange (AO) assay
  - Alcian blue stain
  - Morpholino knockdown
  - *o*-Dianisidine stain
  - Sectioning
  - Immunofluorescence (IF)
  - PGE_2 metabolite quantification
  - cRNA synthesis, microinjections and rescue studies
  - Rescue experiments with $dmPGE_2$
  - qRT-PCR
  - CRISPR-Cas9 mutagenesis
  - Genetic models
  - Image acquisition and phenotype quantification
- QUANTIFICATION AND STATISTICAL ANALYSIS

SUPPLEMENTAL INFORMATION

Supplemental information can be found online at https://doi.org/10.1016/j.isci.2024.111271.

Received: January 10, 2024
Revised: June 30, 2024
Accepted: October 24, 2024
Published: October 28, 2024

REFERENCES

1. Wesselman, H.M., Arceri, L., Nguyen, T.K., Lara, C.M., and Wingert, R.A. (2024). Genetic mechanisms of multiciliated cell development: from fate choice to differentiation in zebrafish and other models. FEBS J. *291*, 4159–4192. https://doi.org/10.1111/febs.17012.
2. Dalton, D., Chadwick, R., and McGinnis, W. (1989). Expression and embryonic function of empty spiracles: a Drosophila homeo box gene with two patterning functions on the anterior-posterior axis of the embryo. Genes Dev. *3*, 1940–1956. https://doi.org/10.1101/gad.3.12a.1940.
3. Walldorf, U., and Gehring, W.J. (1992). Empty spiracles, a gap gene containing a homeobox involved in Drosophila head development. EMBO J. *11*, 2247–2259. https://doi.org/10.1002/j.1460-2075.1992.tb05284.x.
4. Simeone, A., Acampora, D., Gulisano, M., Stornaiuolo, A., and Boncinelli, E. (1992). Nested expression domains of four homeobox genes in developing rostral brain. Nature *358*, 687–690. https://doi.org/10.1038/358687a0.
5. Simeone, A., Gulisano, M., Acampora, D., Stornaiuolo, A., Rambaldi, M., and Boncinelli, E. (1992). Two vertebrate homeobox genes related to the Drosophila empty spiracles gene are expressed in the embryonic cerebral cortex. EMBO J. *11*, 2541–2550. https://doi.org/10.1002/j.1460-2075.1992.tb05319.x.
6. Gulisano, M., Broccoli, V., Pardini, C., and Boncinelli, E. (1996). Emx1 and Emx2 show different patterns of expression during proliferation and differentiation of the developing cerebral cortex in the mouse. Eur. J. Neurosci. *8*, 1037–1050. https://doi.org/10.1111/j.1460-9568.1996.tb01590.x.
7. Miyamoto, N., Yoshida, M., Kuratani, S., Matsuo, I., and Aizawa, S. (1997). Defects of urogenital development in mice lacking Emx2. Development *124*, 1653–1664.
8. Mallamaci, A., Iannone, R., Briata, P., Pintonello, L., Mercurio, S., Boncinelli, E., and Corte, G. (1998). EMX2 protein in the developing mouse brain and olfactory area. Mech. Dev. *77*, 165–172. https://doi.org/10.1016/S0925-4773(98)00141-5.
9. Tole, S., Goudreau, G., Assimacopoulos, S., and Grove, E.A. (2000). Emx2 Is required for growth of the hippocampus but not for hippocampal field specification. J. Neurosci. *20*, 2618–2625. https://doi.org/10.1523/JNEUROSCI.20-07-02618.2000.
10. Cecchi, C. (2002). Emx2: a gene responsible for cortical development, regionalization and area specification. Gene *291*, 1–9. https://doi.org/10.1016/s0378-1119(02)00623-6.
11. Galli, R., Fiocco, R., De Filippis, L., Muzio, L., Gritti, A., Mercurio, S., Broccoli, V., Pellegrini, M., Mallamaci, A., and Vescovi, A.L. (2002). Emx2 regulates the proliferation of stem cells of the adult mammalian central nervous system. Development *129*, 1633–1644. https://doi.org/10.1242/dev.129.7.1633.
12. Kawahara, A., and Dawid, I.B. (2002). Developmental expression of zebrafish emx1 during early embryogenesis. Gene Expr. Patterns *2*, 201–206. https://doi.org/10.1016/s1567-133x(02)00062-5.
13. Schubert, F.R., and Lumsden, A. (2005). Transcriptional control of early tract formation in the embryonic chick midbrain. Development *132*, 1785–1793. https://doi.org/10.1242/dev.01731.
14. Brancaccio, M., Pivetta, C., Granzotto, M., Filippis, C., and Mallamaci, A. (2010). Emx2 and Foxg1 inhibit gliogenesis and promote neuronogenesis. Stem Cell. *28*, 1206–1218. https://doi.org/10.1002/stem.443.
15. Holley, M., Rhodes, C., Kneebone, A., Herde, M.K., Fleming, M., and Steel, K.P. (2010). Emx2 and early hair cell development in the mouse inner ear. Dev. Biol. *340*, 547–556. https://doi.org/10.1016/j.ydbio.2010.02.004.
16. Mariani, J., Favaro, R., Lancini, C., Vaccari, G., Ferri, A.L., Bertolini, J., Tonoli, D., Latorre, E., Caccia, R., Ronchi, A., et al. (2012). Emx2 is a dose-dependent negative regulator of Sox2 telencephalic enhancers. Nucleic Acids Res. *40*, 6461–6476. https://doi.org/10.1093/nar/gks295.
17. Jiang, T., Kindt, K., and Wu, D.K. (2017). Transcription factor Emx2 controls stereociliary bundle orientation of sensory hair cells. Elife *6*, e23661. https://doi.org/10.7554/eLife.23661.
18. Pellegrini, M., Mansouri, A., Simeone, A., Boncinelli, E., and Gruss, P. (1996). Dentate gyrus formation requires Emx2. Development *122*, 3893–3898. https://doi.org/10.1242/dev.122.12.3893.
19. Yoshida, M., Suda, Y., Matsuo, I., Miyamoto, N., Takeda, N., Kuratani, S., and Aizawa, S. (1997). Emx1 and Emx2 functions in development of dorsal telencephalon. Development *124*, 101–111. https://doi.org/10.1242/dev.124.1.101.
20. Brunelli, S., Faiella, A., Capra, V., Nigro, V., Simeone, A., Cama, A., and Boncinelli, E. (1996). Germline mutations in the homeobox gene EMX2 in patients with severe schizencephaly. Nat. Genet. *12*, 94–96. https://doi.org/10.1038/ng0196-94.
21. Faiella, A., Brunelli, S., Granata, T., D'Incerti, L., Cardini, R., Lenti, C., Battaglia, G., and Boncinelli, E. (1997). A number of schizencephaly patients including 2 brothers are heterozygous for germline mutations in the homeobox gene EMX2. Eur. J. Hum. Genet. *5*, 186–190.
22. Granata, T., Farina, L., Faiella, A., Cardini, R., D'Incerti, L., Boncinelli, E., and Battaglia, G. (1997). Familial schizencephaly associated with EMX2 mutation. Neurology *48*, 1403–1406. https://doi.org/10.1212/wnl.48.5.1403.
23. Pang, T., Atefy, R., and Sheen, V. (2008). Malformations of cortical development. Neurol. *14*, 181–191. https://doi.org/10.1097/NRL.0b013e31816606b9.
24. Doostparast Torshizi, A., and Wang, K. (2022). Tissue-wide cell-specific proteogenomic modeling reveals novel candidate risk genes in autism spectrum disorders. NPJ Syst. Biol. Appl. *8*, 31. https://doi.org/10.1038/s41540-022-00243-8.
25. Li, H., Liao, S., Luo, G., Li, H., Wang, S., Li, Z., and Luo, X. (2022). An association between EMX2 variations and Mayer-Rokitansky-Küster-Hauser syndrome: a case-control study of Chinese women. J. Healthc. Eng. *2022*, e9975369. https://doi.org/10.1155/2022/9975369.
26. Ji, Y.R., Warrier, S., Jiang, T., Wu, D.K., and Kindt, K.S. (2018). Directional selectivity of afferent neurons in zebrafish neuromasts is regulated by Emx2 in presynaptic hair cells. Elife *7*, e35796. https://doi.org/10.7554/eLife.35796.
27. Jacobo, A., Dasgupta, A., Erzberger, A., Siletti, K., and Hudspeth, A.J. (2019). Notch-mediated determination of hair-bundle polarity in mechanosensory hair cells of the zebrafish lateral line. Curr. Biol. *29*, 3579–3587.e7. https://doi.org/10.1016/j.cub.2019.08.060.
28. Kozak, E.L., Palit, S., Miranda-Rodríguez, J.R., Janjic, A., Böttcher, A., Lickert, H., Enard, W., Theis, F.J., and López-Schier, H. (2020). Epithelial planar bipolarity emerges from Notch-mediated asymmetric inhibition of Emx2. Curr. Biol. *30*, 1142–1151.e6. https://doi.org/10.1016/j.cub.2020.01.027.
29. Marra, A.N., Adeeb, B.D., Chambers, B.E., Drummond, B.E., Ulrich, M., Addiego, A., Springer, M., Poureetezadi, S.J., Chambers, J.M., Ronshaugen, M., and Wingert, R.A. (2019). Prostaglandin signaling regulates renal multiciliated cell specification and maturation. Proc. Natl. Acad. Sci. USA *116*, 8409–8418. https://doi.org/10.1073/pnas.1813492116.
30. Chambers, J.M., Addiego, A., Flores-Mireles, A.L., and Wingert, R.A. (2020). Ppargc1a controls ciliated cell development by regulating prostaglandin biosynthesis. Cell Rep. *33*, 108370. https://doi.org/10.1016/j.celrep.2020.108370.
31. Wesselman, H.M., Flores-Mireles, A.L., Bauer, A., Pei, L., and Wingert, R.A. (2023). Esrrγa regulates nephron and ciliary development by controlling prostaglandin synthesis. Development *150*, dev201411. https://doi.org/10.1242/dev.201411.
32. Liu, Y., Pathak, N., Kramer-Zucker, A., and Drummond, I.A. (2007). Notch signaling controls the differentiation of transporting epithelia and multiciliated cells in the zebrafish pronephros. Development *134*, 1111–1122. https://doi.org/10.1242/dev.02806.
33. Ma, M., and Jiang, Y.-J. (2007). Jagged2a-notch signaling mediates cell fate choice in the zebrafish pronephric duct. PLoS Genet. *3*, e18. https://doi.org/10.1371/journal.pgen.0030018.
34. Wingert, R.A., Selleck, R., Yu, J., Song, H.-D., Chen, Z., Song, A., Zhou, Y., Thisse, B., Thisse, C., McMahon, A.P., and Davidson, A.J. (2007). The cdx genes and retinoic acid control the positioning and segmentation of the zebrafish pronephros. PLoS Genet. *3*, 1922–1938. https://doi.org/10.1371/journal.pgen.0030189.
35. Chambers, B.E., Weaver, N.E., Lara, C.M., Nguyen, T.K., and Wingert, R.A. (2024). (Zebra)fishing for nephrogenesis genes. Tissue Barriers *12*, 2219605. https://doi.org/10.1080/21688370.2023.2219605.
36. Nguyen, T.K., Petrikas, M., Chambers, B.E., and Wingert, R.A. (2023). Principles of zebrafish nephron segment development. J. Dev. Biol. *11*, 14. https://doi.org/10.3390/jdb11010014.
37. Marra, A.N., Li, Y., and Wingert, R.A. (2016). Antennas of organ morphogenesis: the roles of cilia in vertebrate kidney development. Genesis *54*, 457–469. https://doi.org/10.1002/dvg.22957.
38. Marra, A.N., Chambers, B.E., Chambers, J.M., Drummond, B.E., Adeeb, B.D., Wesselman, H.M., Morales, E.E., Handa, N., Pettini, T., Ronshaugen, M., et al. (2019). Chapter 11 - Visualizing gene expression during zebrafish pronephros development and regeneration. In Methods in Cell Biology Methods in Kidney Cell Biology - Part B, T. Weimbs, ed.

(Academic Press), pp. 183–215. https://doi.org/10.1016/bs.mcb.2019.06.003.
39. Wesselman, H.M., Nguyen, T.K., Chambers, J.M., Drummond, B.E., and Wingert, R.A. (2022). Advances in understanding the genetic mechanisms of zebrafish renal multiciliated cell development. J. Dev. Biol. *11*, 1. https://doi.org/10.3390/jdb11010001.
40. Gokey, J.J., Ji, Y., Tay, H.G., Litts, B., and Amack, J.D. (2016). A Kupffer's vesicle size threshold for robust left-right patterning of the zebrafish embryo. Dev. Dynam. *245*, 22–33. https://doi.org/10.1002/dvdy.24355.
41. Dasgupta, A., and Amack, J.D. (2016). Cilia in vertebrate left–right patterning. Philos. Trans. R. Soc. Lond. B Biol. Sci. *371*, 20150410. https://doi.org/10.1098/rstb.2015.0410.
42. Askary, A., Xu, P., Barske, L., Bay, M., Bump, P., Balczerski, B., Bonaguidi, M.A., and Crump, J.G. (2017). Genome-wide analysis of facial skeletal regionalization in zebrafish. Development *144*, 2994–3005. https://doi.org/10.1242/dev.151712.
43. Yelon, D., Horne, S.A., and Stainier, D.Y. (1999). Restricted expression of cardiac myosin genes reveals regulated aspects of heart tube assembly in zebrafish. Dev. Biol. *214*, 23–37. https://doi.org/10.1006/dbio.1999.9406.
44. Vasilyev, A., Liu, Y., Mudumana, S., Mangos, S., Lam, P.-Y., Majumdar, A., Zhao, J., Poon, K.-L., Kondrychyn, I., Korzh, V., and Drummond, I.A. (2009). Collective cell migration drives morphogenesis of the kidney nephron. PLoS Biol. *7*, e1000009. https://doi.org/10.1371/journal.pbio.1000009.
45. Hatch, K., Pabon, A., and DiMario, J.X. (2017). EMX2 activates slow myosin heavy chain 2 gene expression in embryonic muscle fibers. Mech. Dev. *147*, 8–16. https://doi.org/10.1016/j.mod.2017.06.006.
46. Cha, Y.I., Kim, S.H., Solnica-Krezel, L., and Dubois, R.N. (2005). Cyclooxygenase-1 signaling is required for vascular tube formation during development. Dev. Biol. *282*, 274–283. https://doi.org/10.1016/j.ydbio.2005.03.014.
47. Lord, A.M., North, T.E., and Zon, L.I. (2007). Prostaglandin E2: making more of your marrow. Cell Cycle *6*, 3054–3057. https://doi.org/10.4161/cc.6.24.5129.
48. Fliegauf, M., Benzing, T., and Omran, H. (2007). When cilia go bad: cilia defects and ciliopathies. Nat. Rev. Mol. Cell Biol. *8*, 880–893. https://doi.org/10.1038/nrm2278.
49. Diener, D.R., Lupetti, P., and Rosenbaum, J.L. (2015). Proteomic analysis of isolated ciliary transition zones reveals the presence of ESCRT proteins. Curr. Biol. *25*, 379–384. https://doi.org/10.1016/j.cub.2014.11.066.
50. Sun, S., Fisher, R.L., Bowser, S.S., Pentecost, B.T., and Sui, H. (2019). Three-dimensional architecture of epithelial primary cilia. Proc. Natl. Acad. Sci. USA *116*, 9370–9379. https://doi.org/10.1073/pnas.1821064116.
51. Preble, A.M., Giddings, T.M., and Dutcher, S.K. (2000). Basal bodies and centrioles: their function and structure. Curr. Top. Dev. Biol. *49*, 207–233. https://doi.org/10.1016/s0070-2153(99)49010-6.
52. Corkins, M.E., Krneta-Stankic, V., Kloc, M., and Miller, R.K. (2021). Aquatic models of human ciliary diseases. Genesis *59*, e23410. https://doi.org/10.1002/dvg.23410.
53. Ji, Y.R., Tona, Y., Wafa, T., Christman, M.E., Tourney, E.D., Jiang, T., Ohta, S., Cheng, H., Fitzgerald, T., Fritzsch, B., et al. (2022). Function of bidirectional sensitivity in the otolith organs established by transcription factor Emx2. Nat. Commun. *13*, 6330. https://doi.org/10.1038/s41467-022-33819-3.
54. Lozano-Ortega, M., Valera, G., Xiao, Y., Faucherre, A., and López-Schier, H. (2018). Hair cell identity establishes labeled lines of directional mechanosensation. PLoS Biol. *16*, e2004404. https://doi.org/10.1371/journal.pbio.2004404.
55. Tona, Y., and Wu, D.K. (2020). Live imaging of hair bundle polarity acquisition demonstrates a critical timeline for transcription factor Emx2. Elife *9*, e59282. https://doi.org/10.7554/eLife.59282.
56. Kindt, K.S., Akturk, A., Jarysta, A., Day, M., Beirl, A., Flonard, M., and Tarchini, B. (2021). EMX2-GPR156-Gαi reverses hair cell orientation in mechanosensory epithelia. Nat. Commun. *12*, 2861. https://doi.org/10.1038/s41467-021-22997-1.
57. Jin, D., Ni, T.T., Sun, J., Wan, H., Amack, J.D., Yu, G., Fleming, J., Chiang, C., Li, W., Papierniak, A., et al. (2014). Prostaglandin signaling regulates ciliogenesis by modulating intraflagellar transport. Nat. Cell Biol. *16*, 841–851. https://doi.org/10.1038/ncb3029.
58. Garcia, H., Serafin, A.S., Silbermann, F., Porée, E., Viau, A., Mahaut, C., Billot, K., Birgy, É., Garfa-Traore, M., Roy, S., et al. (2022). Agonists of prostaglandin E2 receptors as potential first in class treatment for nephronophthisis and related ciliopathies. Proc. Natl. Acad. Sci. USA *119*, e2115960119. https://doi.org/10.1073/pnas.2115960119.
59. Katz, S.M., and Morgan, J.J. (1984). Cilia in the human kidney. Ultrastruct. Pathol. *6*, 285–294. https://doi.org/10.3109/01913128409018587.
60. Duffy, J.L., and Suzuki, Y. (1968). Ciliated human renal proximal tubular cells. Observations in three cases of hypercalcemia. Am. J. Pathol. *53*, 609–616.
61. Larsen, T.E., and Ghadially, F.N. (1974). Cilia in lupus nephritis. J. Pathol. *114*, 69–73. https://doi.org/10.1002/path.1711140203.
62. Eymael, J., Willemsen, B., Xu, J., Mooren, F., Steenbergen, E., Wetzels, J.F., Dijkman, H., Jansen, J., Van der Vlag, J., and Smeets, B. (2022). Motile cilia on kidney proximal tubular epithelial cells are associated with tubular injury and interstitial fibrosis. Front. Cell Dev. Biol. *10*, 765887. https://doi.org/10.3389/fcell.2022.765887.
63. Morales, E.E., Handa, N., Drummond, B.E., Chambers, J.M., Marra, A.N., Addiego, A., and Wingert, R.A. (2018). Homeogene emx1 is required for nephron distal segment development in zebrafish. Sci. Rep. *8*, 18038. https://doi.org/10.1038/s41598-018-36061-4.
64. Li, Y., Cheng, C.N., Verdun, V.A., and Wingert, R.A. (2014). Zebrafish nephrogenesis is regulated by interactions between retinoic acid, mecom, and Notch signaling. Dev. Biol. *386*, 111–122. https://doi.org/10.1016/j.ydbio.2013.11.021.
65. Marra, A.N., and Wingert, R.A. (2016). Epithelial cell fate in the nephron tubule is mediated by the ETS transcription factors etv5a and etv4 during zebrafish kidney development. Dev. Biol. *411*, 231–245. https://doi.org/10.1016/j.ydbio.2016.01.035.
66. Bridgewater, D., Cox, B., Cain, J., Lau, A., Athaide, V., Gill, P.S., Kuure, S., Sainio, K., and Rosenblum, N.D. (2008). Canonical WNT/β-catenin signaling is required for ureteric branching. Dev. Biol. *317*, 83–94. https://doi.org/10.1016/j.ydbio.2008.02.010.
67. Okamoto, J., Hirata, T., Chen, Z., Zhou, H.-M., Mikami, I., Li, H., Yagui-Beltran, A., Johansson, M., Coussens, L.M., Clement, G., et al. (2010). EMX2 is epigenetically silenced and suppresses growth in human lung cancer. Oncogene *29*, 5969–5975. https://doi.org/10.1038/onc.2010.330.
68. Boualia, S.K., Gaitan, Y., Murawski, I., Nadon, R., Gupta, I.R., and Bouchard, M. (2011). Vesicoureteral reflux and other urinary tract malformations in mice compound heterozygous for Pax2 and Emx2. PLoS One *6*, e21529. https://doi.org/10.1371/journal.pone.0021529.
69. Boualia, S.K., Gaitan, Y., Tremblay, M., Sharma, R., Cardin, J., Kania, A., and Bouchard, M. (2013). A core transcriptional network composed of Pax2/8, Gata3 and Lim1 regulates key players of pro/mesonephros morphogenesis. Dev. Biol. *382*, 555–566. https://doi.org/10.1016/j.ydbio.2013.07.028.
70. Westerfield, M. (2007). The Zebrafish Book; A guide for the laboratory use of zebrafish (Danio rerio).
71. Kimmel, C.B., Ballard, W.W., Kimmel, S.R., Ullmann, B., and Schilling, T.F. (1995). Stages of embryonic development of the zebrafish. Dev. Dynam. *203*, 253–310. https://doi.org/10.1002/aja.1002030302.
72. Galloway, J.L., Wingert, R.A., Thisse, C., Thisse, B., and Zon, L.I. (2008). Combinatorial regulation of novel erythroid gene expression in zebrafish. Exp. Hematol. *36*, 424–432. https://doi.org/10.1016/j.exphem.2007.11.015.
73. Lengerke, C., Wingert, R., Beeretz, M., Grauer, M., Schmidt, A.G., Konantz, M., Daley, G.Q., and Davidson, A.J. (2011). Interactions between Cdx genes and retinoic acid modulate early cardiogenesis. Dev. Biol. *354*, 134–142. https://doi.org/10.1016/j.ydbio.2011.03.027.
74. Cheng, C.N., Li, Y., Marra, A.N., Verdun, V., and Wingert, R.A. (2014). Flat mount preparation for observation and analysis of zebrafish embryo specimens stained by whole mount in situ hybridization. JoVE *89*, e51604. https://doi.org/10.3791/51604.
75. O'Brien, L.L., Grimaldi, M., Kostun, Z., Wingert, R.A., Selleck, R., and Davidson, A.J. (2011). Wt1a, Foxc1a, and the Notch mediator Rbpj physically interact and regulate the formation of podocytes in zebrafish. Dev. Biol. *358*, 318–330. https://doi.org/10.1016/j.ydbio.2011.08.005.
76. Gerlach, G.F., and Wingert, R.A. (2014). Zebrafish pronephros tubulogenesis and epithelial identity maintenance are reliant on the polarity proteins Prkc iota and zeta. Dev. Biol. *396*, 183–200. https://doi.org/10.1016/j.ydbio.2014.08.038.
77. McCampbell, K.K., Springer, K.N., and Wingert, R.A. (2014). Analysis of nephron composition and function in the adult zebrafish kidney. J. Vis. Exp. *90*, e51644. https://doi.org/10.3791/51644.
78. Kroeger, P.T., Drummond, B.E., Miceli, R., McKernan, M., Gerlach, G.F., Marra, A.N., Fox, A., McCampbell, K.K., Leshchiner, I., Rodriguez-Mari, A., et al. (2017). The zebrafish kidney mutant zeppelin reveals that brca2/fancd1 is essential for pronephros

development. Dev. Biol. *428*, 148–163. https://doi.org/10.1016/j.ydbio.2017.05.025.

79. Tucker, B., and Lardelli, M. (2007). A rapid apoptosis assay measuring relative acridine orange fluorescence in zebrafish embryos. Zebrafish *4*, 113–116. https://doi.org/10.1089/zeb.2007.0508.
80. Neuhauss, S.C., Solnica-Krezel, L., Schier, A.F., Zwartkruis, F., Stemple, D.L., Malicki, J., Abdelilah, S., Stainier, D.Y., and Driever, W. (1996). Mutations affecting craniofacial development in zebrafish. Development *123*, 357–367. https://doi.org/10.1242/dev.123.1.357.
81. Marra, A.N., Ulrich, M., White, A., Springer, M., and Wingert, R.A. (2017). Visualizing multiciliated cells in the zebrafish through a combined protocol of whole mount fluorescent in situ hybridization and immunofluorescence. JoVE *129*, e56261. https://doi.org/10.3791/56261.
82. Hoshijima, K., Jurynec, M.J., Klatt Shaw, D., Jacobi, A.M., Behlke, M.A., and Grunwald, D.J. (2019). Highly efficient CRISPR-Cas9-based methods for generating deletion mutations and F0 embryos that lack gene function in zebrafish. Dev. Cell *51*, 645–657.e4. https://doi.org/10.1016/j.devcel.2019.10.004.
83. Chambers, B.E., Clark, E.G., Gatz, A.E., and Wingert, R.A. (2020). Kctd15 regulates nephron segment development by repressing Tfap2a activity. Development *147*, dev191973. https://doi.org/10.1242/dev.191973.

STAR★METHODS

KEY RESOURCES TABLE

REAGENT or RESOURCE	SOURCE	IDENTIFIER
Antibodies		
Anti-tubulin acetylated	Sigma	T6793; RRID:AB_477585
Anti-γ-tubulin	Sigma	T5192; RRID:AB_261690
Anti-PKC	Santa Cruz	SC216; RRID:AB_2300359
Goat anti-Rabbit IgG (H + L) Highly Cross-Adsorbed Secondary Antibody, Alexa Fluor 594	Invitrogen	A11037; RRID:AB_2534095
Goat anti-Mouse IgG (H + L) Highly Cross-Adsorbed Secondary Antibody, Alexa Fluor 488	Invitrogen	A11029; RRID:AB_138404
Chemicals		
16,16-Dimethyl-prostaglandin E_2	Santa Cruz Biotechnology, Inc	sc-201240
40 kDa Dextran-FITC	Invitrogen	D-1845
Alcian blue 8GX	Fluka Analytical	05500-5G
Acridine Orange hemi (zinc chloride) salt	Sigma	A6014-10G
o-Dianisidine	Sigma	D-9143
Dimethyl Sulfoxide	American Bioanalytical	AB00435-01000
Ethyl Alcohol, Pure	Sigma	E7023-4L
TRIzol® Reagent	Ambion	15596026
N-Phenylthiourea	Sigma	P7629-25G
Commercial Assays		
Prostaglandin E2 Express ELISA Kit	Cayman Chemical	500141
mMESSAGE mMACHINE SP6 Transcription kit	Ambion	AM1340
PerfeCTa SYBR Green SuperMix with ROX	Quantabio	VWR 101414-160
qScript cDNA SuperMix	Quantabio	VWR 101414-106
BtsCI restriction enzyme	New England Biolabs	R0647S
10X NEBuffer 4	New England Biolabs	B7004S
Experimental Models		
emx2$^{el586/el586}$	Askary et al., 2017[42]	ZDB-ALT-171010-8
Oligonucleotides		
emx2 RT-PCR forward CAGCGGCTCTCAGCTATGCAAACTC	This paper	N/A
emx2 RT-PCR reverse GGGCTTTCTTGCTAGAGCATTGTGC	This paper	N/A
emx2 CRISPR forward ACAAAACTTTGGTCTTGGGTGT	This paper	N/A
emx2 CRISPR reverse TTTCTCCGTACAACTGGTCAAA	This paper	N/A
emx2$^{el586/el586}$ forward ACAAAACTTTGGTCTTGGGTGT	This paper	N/A
emx2$^{el586/el586}$ reverse TTGCGAAAAGAGGGTGCG	This paper	N/A
18S qRT-PCR forward TCGGCTACCACATCCAAGGAAGGCAGC	Chambers et al., 2020[30]	N/A

(*Continued on next page*)

Continued

REAGENT or RESOURCE	SOURCE	IDENTIFIER
18S qRT-PCR reverse TTGCTGGAATTACCGCGGCTGCTGGCA	Chambers et al., 2020[30]	N/A
ppargc1a qRT-PCR forward AATGCCAGTGATCAGAGCTGTCCTT	Chambers et al., 2020[30]	N/A
ppargc1a qRT-PCR reverse GTTCTGTGCCTTGCCACCTGGGTAT	Chambers et al., 2020[30]	N/A
ptgs1 qRT-PCR forward CATGCACAGGTCAAAATGAGTT	Chambers et al., 2020[30]	N/A
ptgs1 qRT-PCR reverse TGTGAGGATCGATGTGTTGAAT	Chambers et al., 2020[30]	N/A
emx2 MO splice donor AAACTTACCTTGAAATCTGTGACCC	Gene Tools, LLC	N/A
emx2 MO splice acceptor AGGACTCGTTTCGTTTCCTGCGAAG	Gene Tools, LLC	N/A
emx2 crRNA1 TCGGATCTCGACGATGGCAA	IDT	predesigned guide "AA"
emx2 crRNA2 CCTCAGCGAACACTAAGTCC	IDT	predesigned guide "AC"
emx2 crRNA3 AAGTTGAAGGGTCCCTTTGC	IDT	predesigned guide "AD"
Alt-R ® CRISPR-Cas9 tracrRNA	IDT	1072532
CRISPR Reagents		
Alt-R® S.p. Cas9 Nuclease V3	IDT	1081058
Nuclease Free Duplex Buffer	IDT	11-01-03-01
Accuprime™ *Pfx* SuperMix	Invitrogen	12344–040
QIAquick PCR purification kit	Qiagen	28106
10X NEBuffer 2	New England Biolabs	B7002S
T7 endonuclease I enzyme	New England Biolabs	M0302L
Software		
Prism v 9	GraphPad	https://www.graphpad.com/%20scientificsoftware/prism/
ImageJ	Fiji	ImageJ (https://imagej.nih.gov/ij/)

EXPERIMENTAL MODEL AND STUDY PARTICIPANT DETAILS

The Center for Zebrafish Research at the University of Notre Dame maintained the zebrafish used in these studies and experiments were performed with approval of the University of Notre Dame Institutional Animal Care and Use Committee (IACUC), under protocol numbers 19-06-5412 and 22-07-7335.

ANIMAL MODELS

Tübingen strain zebrafish were used for the reported studies, with the *emx2*$^{el586/el586}$ mutant line propagated on this background. Zebrafish were raised and staged as previously described.[70,71] For all experiments, embryos were incubated in E3 medium at 28°C until the desired developmental stage, anesthetized with 0.02% tricaine, and then fixed using either 4% paraformaldehyde/1x PBS (PFA), or Dent's solution (80% methanol, 20% DMSO).[72] Embryos were analyzed before sex determination, so we cannot report the effect of sex and gender in the context of this study. WISH experiments were performed in triplicate with a sample size of greater than 30 embryos for each replicate. For cilia data analysis, a minimum of 3 samples per experimental group were quantified for each metrics. For cilia length, a minimum of 6 cilia were measured per sample.

METHOD DETAILS

Whole mount *in situ* hybridization (WISH)

WISH was performed as previously described.[72–74] Linearized plasmids were transcribed *in vitro* with T7, T3 or SP6 enzymes to create antisense RNA probes either digoxigenin-labeled (*emx2, odf3b, myl7, slc12a3, slc20a1a, ptgs1, pax2a, jag2b, cetn4, trpm7, slc12a1, cdh17, mecom*) or fluorescein-labeled (*emx2, ppargc1a*) via *in vitro* transcription using IMAGE clone templates as previously described.[34,75,76] All WISH

experiments were performed in triplicate with a sample size of greater than 30 embryos for each replicate. Representative samples were imaged and analyzed.

Dextran-FITC injections

WT and *emx2*$^{el586/el586}$ heterozygous incrosses were incubated in 0.003% *N*-Phenylthiourea (Sigma). At 48 hpf, embryos were anesthetized and 40 kDa Dextran FITC conjugate (5 mg/mL) was injected into the somite to introduce to circulation.[77,78] Embryos were imaged at 6 hpi, 24 hpi and 48 hpi. Mean fluorescent intensity of the head and the pericardium was calculated via ImageJ, and the percentage of remaining fluorescence was calculated using the 6 hpi fluorescent intensity as a baseline.

Acridine Orange (AO) assay

AO experiments were conducted as described.[78,79] AO (Sigma) was prepared by dissolving 50 mg in 50 mL of MilliQ water to create a 100X solution and stored at −20°C, protected from light. AO was diluted in E3 to a 1X working solution before applied to 24 hpf live embryos. Embryos were incubated in AO/E3 for 30 min at room temperature, then washed 3 times for 10 min with E3. Samples were anesthetized in tricaine and imaged in methylcellulose.

Alcian blue stain

Alcian blue staining was conducted as described.[80] At 4 dpf, embryos were fixed in 4% PFA overnight at 4°C in glass vials. They were dehydrated in 100% MeOH at −20°C, then rehydrated. Embryos were bleached at room temperature for 1 h, then rinsed in PBST twice before digested in 1X proteinase K (10 mg/mL) for 15 min, then rinsed twice in PBST again. Afterward, embryos were stained overnight in 0.1% Alcian blue dissolved in 70% ethanol/5% concentrated HCl in glass vials on the rocker. Embryos were then destained using acidic ethanol for 4 h on the rocker, then rinsed twice in PBST and then rehydrated in ethanol series. Embryos were then stored in 100% glycerol for imaging.

Morpholino knockdown

Morpholino oligonucleotides (MO) were designed and obtained from Gene Tools, LLC. MOs were solubilized in DNase/RNase free water to generate 4mM stock solution, which were stored at −20°C. Embryos were injected at one-cell stage with 5 nL of diluted MO. The *emx2* MOs include an *emx2* splice donor 5′-AAACTTACCTTGAAATCTGTGACCC-3′ and *emx2* splice acceptor 5′-AGGACTCGTTTCGTTTCCTGC GAAG-3′. MO specificity was assessed using the reverse transcriptase polymerase chain reaction (RT-PCR) with the following pair of primers 5′-CAGCGGCTCTCAGCTATGCAAACTC-3′ and 5′-GGGCTTTCTTGCTAGAGCATTGTGC-3′. Products were isolated by PCR purification and Sanger Sequencing.

o-Dianisidine stain

o-Dianisidine powder (Sigma) was diluted in 100% ethanol and stored in 4°C. The working solution was prepared as follows: 2 mL of *o*-Dianisidine solution +500 μL Sodium Acetate, pH = 4.5 + 2 mL distilled water +100 μL 30% H_2O_2. The working solution was applied to live embryos at 48 hpf in the dark at room temperature. Then, the reaction was stopped by washing 3X in distilled water, and embryos were then fixed in 4% PFA for imaging.

Sectioning

Sectioning was performed as previously described.[31] Fixed embryos were exposed to 5% and 30% sucrose solution and then incubated with 1:1 solution of 30 sucrose and tissue freezing medium (TFM). Infiltrated samples were embedded in 100% TFM and oriented in Tissue-Tek cryomolds and frozen at - 80°C. 14 μm sections were taken on a Microm HM 550 Cryostat (Thermo Fisher Scientific).

Immunofluorescence (IF)

Whole mount IF experiments were completed as previously described.[29–31,76,81] For cilia, anti-tubulin acetylated diluted 1:400 (Sigma) was used. For basal bodies, anti-γ-tubulin diluted 1:400 (Sigma) was used. For apical membrane, anti-aPKC diluted 1:500 (Santa Cruz) was used.

PGE_2 metabolite quantification

PGE_2 metabolite quantifications were performed according to the manufacturer's protocol (Cayman Chemical, Item No. 500141) and adapted from previously reported studies.[30,31] Groups of 25 WT and *emx2* MO embryos were pooled, anesthetized and flash frozen in 100% ethanol. Lysates were homogenized and the supernatant was isolated after centrifugation at 4°C (15000 rpm for 20 min). The kit reagents and manufacturer supplied protocol was followed for assay completion using a plate reader (SpectraMax ABSPlus) at 420 nm.

cRNA synthesis, microinjections and rescue studies

The *ppargc1a* ORF was cloned into a pUC57 vector flanked by a 5′ KOZAK sequence, Cla1 restriction site and an SP6 promoter region. On the 3′ side, the ORF was followed by a series of STOP codons, an SV40 poly A tail, a NotI restriction site and a T7 promoter region. *ppargc1a* RNA was generated by linearizing with Not1. Linearized plasmid was run off with SP6 RNA polymerase using the mMESSAGE mMACHINE SP6

Transcription kit (Ambion). *ppargc1a* RNA was injected together with *emx2* MO at one-cell stage at concentration 375 pg for rescue study. The *ptgs1* ORF was cloned into a pUC57 vector flanked by a 5′ KOZAK sequence, Cla1 restriction site and an SP6 promoter region. On the 3′ side, the ORF was followed by a series of STOP codons, an SV40 poly A tail, a NotI restriction site and a T7 promoter region. *ptgs1* RNA was generated by linearizing with Not1. Linearized plasmid was run off with SP6 RNA polymerase using the mMESSAGE mMACHINE SP6 Transcription kit (Ambion). *ptgs1* RNA was injected together with *emx2* MO at one-cell stage at concentration 825 pg for rescue study.

Rescue experiments with dmPGE$_2$

Chemical treatments were adapted from previously described studies.[29–31] In short, 16,16-Dimethyl-prostaglandin E$_2$ (Santa Cruz Biotechnology) was dissolved in 100% DMSO (American Bioanalytical) to create 1 M stock. Then 1 M stock was diluted to the treatment dose. Treatments were performed in triplicate with $n > 30$ embryos per replicate.

qRT-PCR

Groups of 30 zebrafish embryos (WT and *emx2* morphants) were pooled at 24 hpf. RNA was extracted using Trizol (Ambion), and cDNA was made from RNA using qScript cDNA SuperMix (QuantaBio). The optimal cDNA concentration was 100 ng for *ppargc1a*, 100 ng for *ptgs1* and 1 ng for 18S controls. PerfeCTa SYBR Green SuperMix with ROX (QuantaBio) was used to complete qRT-PCR. The AB StepOnePlus qRT-PCR machine was used with the following program: 2 min 50°C hold, 10 min 95°C hold, then 35 cycles of 15 s at 95°C (denaturing) and 1 min at 60°C (primer annealing) and product extension steps. Each target and source were completed in three biological replicates and three technical replicates each, with the Ct value normalized to control. Data analysis was performed by using delta delta Ct values comparing WT embryos to the *emx2* morphant embryos, using 18S as a reference gene. The primers used in this study are: *ppargc1a* forward 5′-AATGCCAGTGATCAGAGCTGTCCTT-3′, *ppargc1a* reverse 5′-GTTCTGTGCCTTGCCACCTGGGTAT-3′, *ptgs1* forward 5′-CATGCACAGGTCAAAATGAGTT-3′, *ptgs1* reverse 5′-TGTGAGGATCGATGTGTTGAAT-3′, 18S forward 5′-TCGGCTACCACATCCAAGGAAGGCAGC-3′, 18S reverse 5′-TTGCTGGAATTACCGCGGCTGCTGGCA-3′.

CRISPR-Cas9 mutagenesis

We adapted published methods as follows.[82] In brief, gRNAs targeting the *emx2* coding region were selected using the pre-designed gRNAs from Integrated DNA Technologies (IDT). *emx2* sgRNA 1, *emx2* sgRNA 2, and *emx2* sgRNA 3 targeted different regions in exon 1 of the *emx2* coding frame. Selected crRNA and tracrRNA tools were obtained from IDT and dissolved into 100 μM IDT duplex buffer to make 100 μM stock. To form the crRNA:tracrRNA duplex, we combined a similar amount of cRNA and tracrRNA, vortexed and mixed and performed a rapid heat/cool program using a thermocycler to generate 50 μM duplex solution. To prepare 25 μM Cas9 stock solution, we obtained Cas9 protein from IDT and adjusted to 25 μM stock solution in 20 mM HEPES-NaOH (pH = 7.5), 350 mM KCl, 20% glycerol and dispensed in aliquots and stored at −80°C. To prepare 5 μM cRNA:tracrRNA:Cas9 RNP complex, the crRNA:tracrRNA duplex was first diluted 1:1 with IDT duplex buffer. Then the following injection mix was prepared: 1 μL 25 μM crRNA:tracrRNA (crRNA 1) + 1 μL 25 μM crRNA:tracrRNA (crRNA 2)+1 μL 25 μM crRNA:tracrRNA (crRNA 2) + 1 μL 25 μM Cas9 protein+2 μL nuclease-free water. The injection mix was incubated at 37°C for 5 min, then injected to the one-cell stage embryos with 3 nL. Crispants were identified by performing PCR with the following primers flanking the mutation site: forward 5′-ACAAAACTTTGGTCTTGGGTGT-3′ and reverse 5′-TTTCTCCGTACAACTGGTCAAA-3′. Primers were designed using CHOPCHOP web-based tool (https://chopchop.cbu.uib.no/) to flank all three sgRNA target sites in exon 1, respectively (Figure S3A). In brief, DNA was prepared from individual animals and Accuprime *Pfx* SuperMix (Invitrogen) was used to amplify target sites. PCR products were purified using the QIAquick PCR purification kit (Qiagen) and sent to Notre Dame Genomics Core for sequencing analysis. Additionally, T7 endonuclease assay was used to confirm genome editing, adapted from the method previously described.[83] Purified PCR product (~300 ng), 2 μL 10X NEBuffer 2 (New England Biolabs) and nuclease-free water (total of 20 μL) were mixed and rehybridized using the following program: 5 min at 95°C, ramp down to 85 °C at 2 °C/s, ramp down to 25 °C at 0.1 °C/s, and 25°C for 10 min. Rehybridized products were incubated with 1.5 μL T7 endonuclease I enzyme (New England Biolabs) at 37°C for 1 h and separated on 1.5% agarose gel.

Genetic models

The *emx2*$^{el586/el586}$ mutant line was obtained from Lindsey Barske (Cincinnati Children's Hospital, Ohio).[42] Mutant embryos and heterozygous adults were identified by performing PCR with the following primers flanking the mutation site: forward 5′-ACAAAACTTTGGTCTTGGGTGT-3′, and reverse 5′-TTGCGAAAAGAGGGTGCG-3′. PCR products were purified using the QIAquick PCR purification kit (Qiagen) and sent to Notre Dame Genomics Core for sequencing analysis. Additionally, restriction enzyme digest assay with BtsCI (New England Biolabs) was performed to identify WT, heterozygous or mutant samples. The PCR products (~300 ng) were incubated with 2 μL 10X NEBuffer 4 (New England Biolabs), 1 μL BtsCI restriction enzyme, and nuclease-free water for a total of 20 μL. The mixture was incubated at 50°C for 1 h, and separated on 2% agarose gel.

Image acquisition and phenotype quantification

A Nikon Eclipse Ni with a DS-Fi2 camera was utilized to take pictures of WISH samples and live imaging of zebrafish. WISH segment length was quantified using the Nikon Elements software polyline tool. To mount live embryos, methylcellulose with trace amounts of tricaine was

used. IF images were acquired using a Nikon A1R confocal microscope. For WISH pictures, images were taken at 4X, 10X, 40X and 60X. For live imaging, images were taken at 3X, 8X and 10X. For IF images, images were taken at 60X.

QUANTIFICATION AND STATISTICAL ANALYSIS

ImageJ/Fiji software tool was used to quantify cilia phenotypes. Measurements were performed on samples imaged at 60× magnification. Counting was performed using the multi-point tool. Segment line tool was used for measuring lengths. Cilia length was measured in both proximal and distal domains. A minimum of 6 cilia were measured per sample, and minimum of 3 samples were quantified. Measuring fluorescent intensity was performed using the plot profile function. Each experiment was completed in a minimum of triplicate. From measurements, an average and standard deviation (s.d.) were calculated, and either one-way ANOVA or unpaired t-tests were completed to compare between WT and experimental groups via GraphPad Prism 9 software. Statistical details for each experiment are located in the figure legends.